frontiers in Molecular Neuroscience

ORIGINAL RESEARCH
published: 08 August 2018
doi: 10.3389/fnmol.2018.00193

Mechanisms Underlying the Strong Inhibition of Muscle-Type Nicotinic Receptors by Tetracaine

Raúl Cobo[1], *Magdalena Nikolaeva*[2], *Armando Alberola-Die*[1], *Gregorio Fernández-Ballester*[2], *José M. González-Ros*[2], *Isabel Ivorra*[1] and *Andrés Morales*[1]*

[1] División de Fisiología, Departamento de Fisiología, Genética y Microbiología, Universidad de Alicante, Alicante, Spain,
[2] Instituto de Biología Molecular y Celular, Universidad Miguel Hernández, Alicante, Spain

Nicotinic acetylcholine (ACh) receptors (nAChRs) are included among the targets of a variety of local anesthetics, although the molecular mechanisms of blockade are still poorly understood. Some local anesthetics, such as lidocaine, act on nAChRs by different means through their ability to present as both charged and uncharged molecules. Thus, we explored the mechanisms of nAChR blockade by tetracaine, which at physiological pH is almost exclusively present as a positively charged local anesthetic. The nAChRs from *Torpedo* electroplaques were transplanted to *Xenopus* oocytes and the currents elicited by ACh (I_{ACh}s), either alone or co-applied with tetracaine, were recorded. Tetracaine reversibly blocked I_{ACh}, with an IC_{50} (i.e., the concentration required to inhibit half the maximum I_{ACh}) in the submicromolar range. Notably, at very low concentrations (0.1 μM), tetracaine reduced I_{ACh} in a voltage-dependent manner, the more negative potentials produced greater inhibition, indicating open-channel blockade. When the tetracaine concentration was increased to 0.7 μM or above, voltage-independent inhibition was also observed, indicating closed-channel blockade. The I_{ACh} inhibition by pre-application of just 0.7 μM tetracaine before superfusion of ACh also corroborated the notion of tetracaine blockade of resting nAChRs. Furthermore, tetracaine markedly increased nAChR desensitization, mainly at concentrations equal or higher than 0.5 μM. Interestingly, tetracaine did not modify desensitization when its binding within the channel pore was prevented by holding the membrane at positive potentials. Tetracaine-nAChR interactions were assessed by virtual docking assays, using nAChR models in the closed and open states. These assays revealed that tetracaine binds at different sites of the nAChR located at the extracellular and transmembrane domains, in both open and closed conformations. Extracellular binding sites seem to be associated with closed-channel blockade; whereas two sites within the pore, with different affinities for tetracaine, contribute to open-channel blockade and the enhancement of desensitization, respectively. These results demonstrate a concentration-dependent heterogeneity of tetracaine actions on nAChRs, and contribute to a better understanding of the complex modulation of muscle-type nAChRs by local anesthetics. Furthermore, the combination of functional and virtual assays to decipher nAChR-tetracaine interactions has allowed us to tentatively assign the main nAChR residues involved in these modulating actions.

Keywords: tetracaine, nicotinic acetylcholine receptors, *Xenopus* oocytes, microtransplanted receptors, desensitization, mechanisms of blockade

OPEN ACCESS

Edited by:
Alexandre Mourot,
Université Pierre et Marie Curie, France

Reviewed by:
Alexey Rossokhin,
Scientific Center of Neurology, Russia
Angelo Keramidas,
The University of Queensland, Australia

***Correspondence:**
Andrés Morales
andres.morales@ua.es

Received: *12 February 2018*
Accepted: *15 May 2018*
Published: *08 August 2018*

Citation:
Cobo R, Nikolaeva M, Alberola-Die A, Fernández-Ballester G, González-Ros JM, Ivorra I and Morales A (2018) Mechanisms Underlying the Strong Inhibition of Muscle-Type Nicotinic Receptors by Tetracaine. Front. Mol. Neurosci. 11:193. doi: 10.3389/fnmol.2018.00193

INTRODUCTION

The muscle-type nicotinic acetylcholine (ACh) receptor (nAChR) is the prototypical member of the Cys-loop family of ligand-gated ion channels. This receptor is a heteropentameric protein that is highly expressed by muscle fibers at the neuromuscular junction, and it is composed of $2\alpha_1$, β_1, δ, and ε (substituted by γ during fetal life or in denervated fibers) subunits that are arranged to form a central channel pore (Albuquerque et al., 2009). From a functional point of view, nAChRs are key elements for striated-muscle activation by motoneurons, and thus, for executing voluntary movements. The nAChRs are also expressed in both the central and peripheral nervous systems, and even in non-neuronal tissues, such as astrocytes, keratinocytes, lymphoid cells, lung epithelial cells, and vascular smooth muscle and endothelial cells (Gotti and Clementi, 2004). Although all nAChRs share many structural properties, neuronal nAChRs differ from their muscle-type counterparts in the large diversity of their subunit compositions, which in some cases are tissue specific, and in the associated heterogeneity of their physiological and pharmacological properties (Albuquerque et al., 2009; Taly et al., 2009). Remarkably, these receptors constitute a key therapeutic target, given the high prevalence and relevance of disorders related to nAChR dysfunction, including some myasthenias, addictive behaviors, some types of epilepsy, schizophrenia, Parkinson's and Alzheimer's diseases, inflammation, pain, and even cancer (Hurst et al., 2013; Wu et al., 2015; Parikh et al., 2016; Schulte et al., 2016). Therefore, over the last few decades, much effort has been devoted to understand the mechanisms underlying nAChR modulation, as a large number of highly different molecules affect their functional properties, enabling these receptors to act as allosteric proteins (Changeux, 2014).

Local anesthetics (LAs) are listed among the molecules known to inhibit nAChR activity, including some that are widely used in clinical practice, such as lidocaine (Steinbach, 1968; Wang et al., 2010; Alberola-Die et al., 2011), procaine (Katz and Miledi, 1975; Adams, 1977; Gage and Wachtel, 1984), tetracaine (Ttc) (Koblin and Lester, 1979; Gallagher and Cohen, 1999; Gentry and Lukas, 2001), bupivacaine (Ikeda et al., 1984), benzocaine (Koblin and Lester, 1979; Ogden et al., 1981), adiphenine, and proadifen (Gentry and Lukas, 2001; Spitzmaul et al., 2009). Most LAs seem to be able to inhibit nAChRs; however, there are marked differences among their molecular structures and potencies for nAChR blockade, suggesting that they might not bind to the same modulating sites on these receptors, which would explain their heterogeneous actions on nAChRs. Notably, we have found that lidocaine exerts multiple inhibitory actions on muscle- and neuronal-type nAChRs (Alberola-Die et al., 2011, 2013). Furthermore, most actions of lidocaine on the muscle-type nAChR can be ascertained by using structural analogs of either its hydrophilic (diethylamine; DEA) or hydrophobic (dimethylaniline; DMA) moieties (Alberola-Die et al., 2016a,b). The polar, charged DEA is responsible for the voltage-dependent blockade of nAChRs. DEA also elicits closed-channel blockade, mainly through its action on residues at the extracellular domain (ECD) (Alberola-Die et al., 2016a). In contrast, nAChR blockade by the uncharged, hydrophobic DMA is voltage-independent (although it can bind to the open-channel pore), and it mainly occurs through interactions outside the pore both at the ECD and, preferentially, at inter-subunit crevices on the transmembrane-spanning domain (TMD) to elicit closed-channel blockade. Moreover, DMA enhances nAChR desensitization (Alberola-Die et al., 2016b).

As a long-lasting amino-ester anesthetic, Ttc (2-(dimethylamino)ethyl 4-(butylamino)benzoate) is widely used in topical preparations, as well as spinal anesthesia and plexus/major nerve blocks, especially when a long duration of anesthesia is required. Similar to lidocaine, Ttc belongs to the group of LAs (Arias, 1999) that possess a single aromatic ring (see **Figure 1A**). However, it also has an ester group that is linked to an aliphatic chain that ends in a tertiary amine, which at pH 7, is largely protonated. Besides blocking voltage-dependent Na^+ channels, Ttc has inhibitory effects on muscle (Gallagher and Cohen, 1999; Middleton et al., 1999) and neuronal nAChRs (Gentry and Lukas, 2001), as well as on high-voltage-activated calcium channels (Sugiyama and Muteki, 1994), ryanodine receptors (Zucchi and Ronca-Testoni, 1997), and acid-sensing ion channels (ASICs) (Leng et al., 2013). However, the mechanisms underlying the effects of Ttc on nAChRs remain largely unknown. Since some LAs with amine groups act on nAChRs by different mechanisms and the heterogeneity of their actions are, at least partially, related to the equilibrium between charged and uncharged forms, we have now explored the mechanisms of nAChR blockade by Ttc. Considering its pK_a of 8.4 (Chemicalize, https://chemicalize.com/), almost 97% of Ttc molecules are in a charged form at the recording pH (pH = 7.0). Notably, we found that Ttc induced a much stronger blockade of muscle-type nAChRs than either lidocaine or its charged hydrophilic moiety, DEA. We have now discovered that a roughly homogeneous pool of Ttc molecules elicit both open- and closed-channel blockade and markedly increase nAChR desensitization. These heterogeneous effects of Ttc on nAChRs are mediated by its interaction with different nAChR residues, located at both the ECD and the TMD.

Preliminary results have been published elsewhere in an abstract form (Cobo et al., 2014).

Abbreviations: ACh, acetylcholine; ANR, normal Ringer solution with atropine; DEA, diethylamine; DMA, 2,6-dimethylaniline; EC, extracellular; I_{ACh}, ACh-elicited current; IC, intracellular; I_p, I_{ACh} amplitude at the peak; I_{ss}, I_{ACh} amplitude at the steady-state; LA, local anesthetic; MS-222, ethyl 3-aminobenzoate methanesulfonate; *n*, number of oocytes; *N*, number of oocyte-donor frogs; nAChR, nicotinic acetylcholine receptor; NR, normal Ringer solution; TM, transmembrane spanning-segment; Ttc, tetracaine.

MATERIALS AND METHODS

Purification and Reconstitution of nAChRs

The nAChRs from *Torpedo marmorata* electroplaques were purified by bromoacetylcholine-affinity chromatography in the presence of asolectin lipids, using cholate as a detergent. After elution with carbamylcholine, purified receptors were

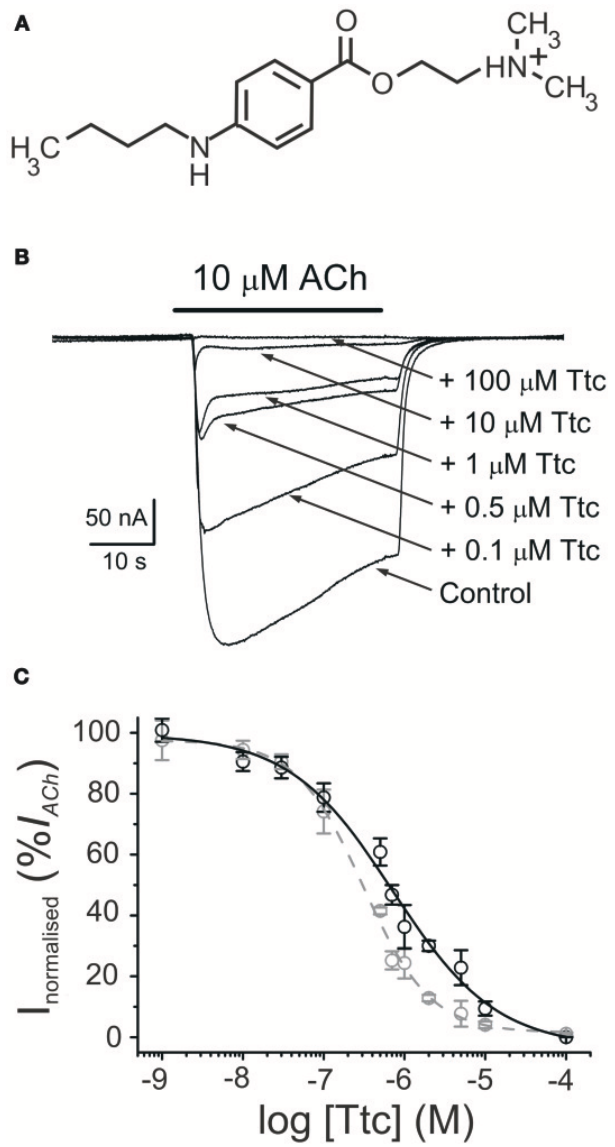

FIGURE 1 | Tetracaine (Ttc) inhibition of currents elicited by ACh (I_{ACh}s). **(A)** Molecular structure of Ttc, showing the amine group largely charged at the recording pH. **(B)** Superimposed I_{ACh}s elicited by 10 μM ACh either alone (Control) or co-applied with different Ttc concentrations, as stated on the right. Note that I_{ACh} decay was accelerated at Ttc concentrations of 0.5 μM or higher. Unless otherwise stated, the holding potential was −60 mV, downward deflections represent inward currents and the bars above the recordings indicate the timing of drug application. **(C)** Ttc concentration-I_{ACh} inhibition relationship. Peak (I_p; black symbols) and steady state (I_{ss}, measured 20 s after the peak; gray symbols) I_{ACh} amplitudes elicited in the presence of Ttc were normalized to the I_{ACh} evoked by ACh alone (Control) and represented against the logarithm of Ttc concentration. Solid and dashed lines are sigmoid curves fitted to I_p and I_{ss} data, respectively. Note that both curves overlap up to 0.1 μM Ttc. Error bars indicate SEM. Each point is the average of 4–23 oocytes from 3 to 11 frogs.

dialyzed and reconstituted in asolectin lipids at a final protein concentration of 0.3–1.2 mg/mL. Samples were aliquoted and stored in liquid nitrogen (Ivorra et al., 2002).

Oocyte Preparation and Microinjection

Adult female *Xenopus laevis* (purchased from Harlan Interfauna Ibérica S.L., Barcelona, Spain; and Centre National de la Recherche Scientifique, Montpellier, France) were immersed in cold 0.17% tricaine methanesulfonate (MS-222) for 20 min, and a piece of the ovary was drawn out aseptically. Animal handling was carried out in accordance with the guidelines for the care and use of experimental animals adopted by the European Union, and the animal protocol was approved by the Ethics Committee of Universidad de Alicante. Stage V and VI oocytes were isolated and their surrounding layers were removed manually. Cells were kept at 15–16°C in a modified Barth's solution (88 mM NaCl, 1 mM KCl, 2.40 mM $NaHCO_3$, 0.33 mM $Ca(NO_3)_2$, 0.41 mM $CaCl_2$, 0.82 mM $MgSO_4$, 10 mM 2-[4-(2-hydroxyethyl)piperazin-1-yl]ethane-1-sulfonic acid (HEPES; pH 7.4), 100 U/mL penicillin, and 0.1 mg/mL streptomycin) until further use. Oocytes were microinjected with 100 nL of an aliquot of reconstituted nAChRs (Morales et al., 1995).

Two-Electrode Voltage-Clamp Recordings in Oocytes

Membrane current recordings were performed at 21–25°C, 16–72 h after injection of proteoliposomes, using a high-compliance two-microelectrode voltage-clamp system (TurboTEC-10CD, npi Tamm, Germany). The recording methodology has been previously described (Morales et al., 1995; Alberola-Die et al., 2016b). Briefly, oocytes were placed in a 150-μL recording chamber and continuously superfused with normal frog Ringer's solution (NR: 115 mM NaCl, 2 mM KCl, 1.8 mM $CaCl_2$, 5 mM HEPES, pH 7.0) supplemented with 0.5 μM atropine sulfate (normal Ringer with atropine, ANR) to block any muscarinic response (Kusano et al., 1982). The membrane potential was held at −60 mV, unless otherwise specified. Oocytes were superfused with ACh and the other drugs under investigation that had been diluted in ANR solution. Superfusion of the oocytes was conducted at a flow rate of 13–17 mL/min. Membrane currents elicited by ACh (I_{ACh}), either alone or co-applied with Ttc, were low-pass filtered at 30–1,000 Hz, after sampling at fivefold the filter frequency (Digidata series 1550 and 1440 A; Axon Instruments, Foster City, CA, USA), as recorded on two PC-computers using the WCP v. 4.8.6. package developed by J. Dempster (Strathclyde Electrophysiology Software, University of Strathclyde, Scotland, UK) and AxoScope v. 10.0.0.60 software (Molecular Devices Corporation, Sunnyvale, CA, USA).

Experimental Design

Experimental procedures were similar to those used to study the effects of lidocaine (Alberola-Die et al., 2011) and other modulators (Alberola-Die et al., 2016a,b) on nAChRs. Briefly, the Ttc concentration-I_{ACh} inhibition relationship was determined by measuring I_{ACh}s evoked by 10 μM ACh alone, or together with different concentrations of Ttc. For the competition assays, ACh concentration-I_{ACh} amplitude curves were obtained by bathing injected oocytes with increasing concentrations of ACh, either alone or together with 0.7 μM Ttc. The I_{ACh}s were normalized

to the maximum I_{ACh} evoked by ACh alone, and the values were fitted to a sigmoid curve (see Equation 3 below). To allow nAChRs to recover from desensitization, the interval between consecutive ACh applications was at least 5 min. To assess the blockade of resting nAChRs by Ttc, we compared the I_{ACh}s elicited by ACh (from 1 μM to 1 mM) alone, or co-applied with 0.7 μM Ttc, either directly, or after 12 s of Ttc pre-application (at the same concentration). To better characterize the effects of Ttc on nAChR desensitization and compare I_{ACh} deactivation in the presence and the absence of Ttc, in some experiments, the oocyte remained superfused with Ttc (at 0.1 or 0.7 μM) for 12 s after withdrawal of 100 μM ACh.

Voltage dependence of the I_{ACh} blockade by Ttc was assessed by: (i) applying a series of 800 ms voltage pulses (from −120 to +60 mV, in 20 mV steps) to the oocyte before ligand superfusion and during the I_{ACh} plateau elicited by 10 μM ACh, either alone, or co-applied with different concentrations of Ttc; the −120 mV pulse duration was extended up to 1500 ms to allow a more complete current relaxation. (ii) From a holding potential of −60 mV, applying a single 800 ms voltage pulse to either +40 or +60 mV during the I_{ACh} plateau elicited by 10 μM ACh, either alone, or when co-applied with 0.1 or 0.7 μM Ttc. (iii) Comparing the I_{ACh} blockade induced by co-application of 0.7 μM Ttc with 10 μM ACh, to the effect when 0.7 μM Ttc was just pre-applied or administered with a combined pre- and co-application, while holding the membrane potential either at −60 or +40 mV.

Data Analysis and Statistical Procedures

Inhibition curves were determined by measuring the I_{ACh} evoked by 10 μM ACh in the presence of different concentrations of Ttc. The I_{ACh}s (both at the peak and 20 s after) elicited in the presence of Ttc were normalized to the I_{ACh} evoked by ACh alone. Data were fitted to a logistic curve with the Origin 6.1 software (OriginLab Corp. Northampton, MA, U.S.A.), using the following Equation (1):

$$I_{ACh+Ttc} = \left(\frac{I_{ACh}max - I_{ACh}min}{1 + ([Ttc]/IC_{50})^{n_H}} \right) + I_{ACh}min$$

where $I_{ACh+Ttc}$ is the I_{ACh} amplitude elicited by co-application of 10 μM ACh with Ttc at a given concentration ([Ttc]); $I_{ACh}max$ and $I_{ACh}min$ are the maximum and minimum I_{ACh}s recorded, respectively; IC_{50} is the Ttc concentration required to inhibit half the maximum I_{ACh}; and n_H is the Hill coefficient.

The rate of desensitization was determined from the I_{ACh} decay elicited by ACh (10 or 100 μM), either alone, or co-applied with different concentrations of Ttc (0.1–2 μM). The time constant of the I_{ACh} decay was obtained through fitting to an exponential decay curve using the OriginPro 8 software (OriginLab Corp. Northampton, MA, U.S.A.). In addition, based on the methods of Sobolevsky et al. (1999), the change in the rate of desensitization induced by Ttc (0.01–2 μM) was determined using the following Equation (2):

$$I_{ACh}\ desensitization\ change = \left(\frac{I_{ss\_Ttc}/I_{p\_Ttc}}{I_{ss\_Ctr}/I_{p\_Ctr}} \right)$$

where I_{p_Ctr} and I_{p_Ttc} are the I_{ACh} peaks elicited by ACh (10 or 100 μM) either alone, or together with Ttc, respectively; I_{ss_Ctr} and I_{ss_Ttc} are I_{ACh}s 20 s after the corresponding I_{ACh} peaks.

To characterize the pharmacological profile of Ttc, nAChRs were activated by different concentrations of ACh alone, or co-applied with Ttc, at roughly its IC_{50}, either directly, or after its pre-application for 12 s. Dose-response data were fitted to the following form of the Hill Equation (3):

$$\frac{I}{I_{ACh}max} = \left[1 + \left(\frac{EC_{50}}{[ACh]} \right)^{n_H} \right]^{-1}$$

where I is the I_{ACh} amplitude elicited at a given concentration of ACh ([ACh]) applied either alone, or together with Ttc; EC_{50} is the agonist concentration required to obtain one-half the maximum I_{ACh}; and $I_{ACh}max$ and n_H are as in Equation (1).

Net *i/v* curves for I_{ACh} were obtained by subtracting, for each voltage, the steady state currents attained in ANR (measured during the last 100 ms of the pulse) from the corresponding currents recorded in the presence of 10 μM ACh alone, or together with Ttc. These net I_{ACh} values were normalized, for each oocyte, to the ACh response at −60 mV.

Unless otherwise specified, values presented were the mean ± standard error of the mean (SEM); "*n*" indicates the number of oocytes and "*N*" is the number of oocyte-donor frogs from which the data were obtained. When comparing two-group means of normally distributed values, the Student's *t*-test was used; otherwise, the Mann–Whitney rank-sum test was applied. Among-group differences were determined by the analysis of variance (ANOVA), and mean differences for each pair of groups were determined with the Bonferroni *t*-test. The one-sample *t*-test was used to compare the mean of an experimental group with a specified value. For the comparison of EC_{50} and IC_{50} values, we used the confidence intervals (CIs) computed by the curve-fitting function of the Origin 6.1 software, using 95% confidence levels. The criterion of "non-overlapping 95% confidence intervals" was used to determine significant differences. A significance level of $p < 0.05$ was considered in all cases.

Virtual Docking Assays

Docking assays were carried out as previously described (Alberola-Die et al., 2016a,b). Briefly, *Torpedo* nAChR structures in the closed (4 Å resolution, pdb code 2BG9; Unwin, 2005) and open (6.2 Å resolution, pdb code 4AQ9; Unwin, 1995; Unwin and Fujiyoshi, 2012), were obtained from the Research Collaboratory for Structural Bioinformatics (RCSB) Protein Data Bank (PDB). The specific edition of the protein was made using DeepView v4.1 (Guex and Peitsch, 1997) and Yasara (Krieger et al., 2002, 2004) software without further optimization. The structure of Ttc was obtained from the National Center for Biotechnology Information (NCBI) PubChem database (http://www.ncbi.nlm.nih.gov/pccompound). A global docking procedure was accomplished with AutoDock 4 (Morris et al., 2008)

implemented in Yasara, in which a total of 800 flexible docking runs were set and clustered around the putative binding sites. The program then performed a simulated annealing minimization of the complexes, which moved the structure to a nearby stable energy minimum, by using the implemented (Assisted Model Building with Energy Refinement) AMBER 99 force field (Duan et al., 2003). The Yasara pH command was set to 7.0, to ensure that molecules preserved their pH dependency of bond orders and protonation patterns. In this way, 97% of the Ttc molecules were protonated. The best binding energy complex in each cluster was stored, analyzed, and used to select the best orientation of the interacting partners.

Global docking of Ttc on the nAChR channel pore systematically occurred at a single, high-affinity binding site. Thus, no other sites were found, following this strategy. In order to explore alternative binding sites with lower affinities within the pore, the high-affinity site was blocked with a Ttc molecule before starting subsequent docking runs. We used the best position of Ttc bound to the deep residues within the pore. In this way, we ensured that the high-affinity site was already occupied, and simulated a scenario with a high concentration of Ttc. Figures were drawn with open source PyMol (The PyMOL Molecular Graphics System, Version 1.8 Schrödinger, LLC, at http://www.pymol.org/).

The theoretical affinities of Ttc at its binding site can be determined by calculating the binding energy of the ligand-receptor complex. The binding energy is obtained by measuring the energy at infinite distance (the unbound state) and subtracting from that value the energy of the complex (the bound state). The relationship between the Gibbs free energy of binding (ΔG, cal/mol) and the dissociation constant (K_d) was determined by the following Equation (4):

$$\Delta G = -RT \ln K_d$$

where $R = 1.98$ cal/molK and $T = 298$ K. Thus, the more positive the binding energy, the more favorable the interaction in the context of the chosen force field.

Drugs

The drugs ACh, atropine sulfate, Ttc, MS-222, penicillin, and streptomycin were obtained from Sigma (St. Louis, MO, USA), and HEPES was obtained from Acros Organics (New Jersey, NJ, USA). The reagents of general use were purchased from Scharlau Chemie SA (Barcelona, Spain). All solutions were made in ANR just before each application.

RESULTS

Inhibition of I_{ACh} by Ttc

The superfusion of Ttc (see chemical structure in **Figure 1A**) on either uninjected oocytes or those bearing nAChRs, with the membrane potential clamped at −60 mV, did not modify their cell membrane conductance, even at concentrations as high as 1 mM. In contrast, co-application of 10 μM ACh with 1 nM−100 μM Ttc reversibly inhibited I_{ACh}, in a dose-dependent manner (**Figure 1B**). The IC_{50} and n_H values (see Equation 1) for the I_{ACh} peak (I_p) were 0.7 μM (95% CI, 0.5–0.9 μM; n = 4–23, N = 3–11) and 0.7 ± 0.1, respectively (black circles and continuous line; **Figure 1C**). At low Ttc concentrations (up to 0.1 μM), this I_p inhibition was similar to that measured 20 s after I_p, which will be referred to hereafter as the "steady state current" (I_{ss}). However, at Ttc concentrations higher than 0.1 μM, the I_{ss} blockade was significantly greater than the corresponding I_p inhibition (see **Figure 1B**). Thus, the dose-inhibition curve for the I_{ss} showed an IC_{50} of 0.3 μM (95% CI, 0.2–0.4 μM, same cells and donor frogs as above) and a slope of 1.0 ± 0.1 (gray circles and dashed line; **Figure 1C**). Interestingly, the effects of Ttc on muscle-type nAChR was specific, as gamma-aminobutyric acid ($GABA_A$) receptors ($GABA_A$Rs), which also belong to the Cys-loop family of receptors, were not noticeably affected by Ttc, even at concentrations of 100-fold the IC_{50} of Ttc on I_{ACh} (see **Figure S1**).

Voltage Dependence of nAChR Blockade by Ttc

To elucidate whether I_{ACh} inhibition by Ttc is voltage-dependent, voltage pulses were applied to oocytes while superfusing them with ANR, or during the I_{ACh} plateau elicited by 10 μM ACh, either alone, or together with 0.1 or 0.7 μM Ttc (**Figures 2A$_1$,A$_2$**, respectively; see Experimental design in Material and methods). The *i/v* curves of net I_{ACh}*s* elicited by ACh, either alone, or co-applied with 0.1 or 0.7 μM Ttc, showed that neither I_{ACh} reversal potential, close to 0 mV, nor its inward rectification were affected by the presence of Ttc (**Figures 2B$_1$,B$_2$**; see also Morales et al., 1995). However, co-application of 10 μM ACh with 0.1 μM Ttc reduced I_{ACh} amplitude in a voltage-dependent manner; thus, the more hyperpolarized the membrane potential, the larger the blockade (**Figure 2B$_1$**). This suggests that Ttc, at this concentration, mainly binds within the channel pore.

An additional mechanism of blockade was present when 0.7 μM Ttc was co-applied with ACh, which roughly accounted for 35% of I_{ACh} inhibition at positive potentials (**Figure 2B$_2$**). It ought to be considered that positive potentials should eject the positively charged Ttc from the channel pore. Therefore, this added I_{ACh} inhibition seems voltage-independent, indicating that at concentrations close to the IC_{50}, Ttc also interacts with nAChR residues located outside the pore. Nonetheless, the voltage-dependent blockade of I_{ACh} remained at 0.7 μM Ttc (compare the extent of I_{ACh} blockade at negative *versus* positive potentials in **Figure 2B$_2$**; see also **Figure S2**, which plots the I_{ACh} remnant vs. membrane potential when ACh was co-applied with different concentrations of Ttc). This voltage-dependent inhibition facilitates the estimation of the apparent rate of channel pore blockade. Thus, during the I_{ACh} plateau elicited by 10 μM ACh in the presence of 0.1 or 0.7 μM Ttc, the membrane potential was stepped back to −60 mV, after an 800 ms pulse at either +40 or +60 mV, (**Figure 2C$_1$**). As shown in **Figure 2C$_2$**, I_{ACh} blockade at −60 mV followed an exponential function with time constant values of 749 ± 32 ms (n = 10, N = 3) and 332 ± 25 ms (n = 11; N = 4) for 0.1 and 0.7 μM Ttc, respectively.

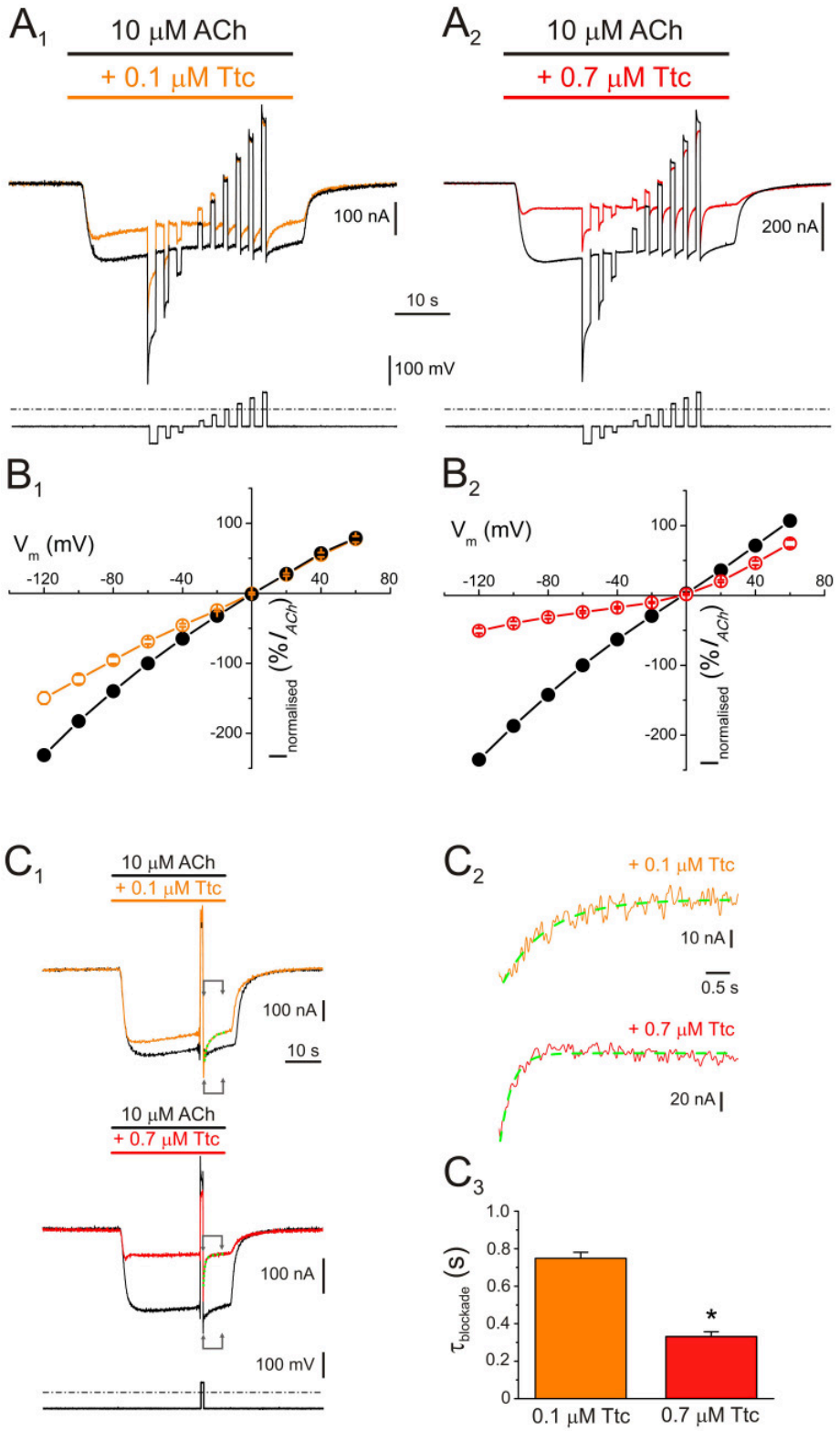

FIGURE 2 | Voltage dependence of nicotinic acetylcholine receptor (nAChR) blockade by tetracaine (Ttc). **(A)** I_{ACh}s (upper traces) elicited by 10 μM ACh either alone (**A_1**,**A_2**, black recordings), or in the presence of 0.1 μM (**A_1**, orange), or 0.7 μM Ttc (**A_2**, red) when the voltage protocol, indicated below the currents, was applied. **(B)** Plots of net *i/v* relationships for I_{ACh}s evoked, following the protocol shown in **A**. Control I_{ACh}s are represented by black symbols and lines **(B_1,B_2)**, whereas those

(Continued)

FIGURE 2 | evoked in the presence of 0.1 μM (**B_1**) and 0.7 μM Ttc (**B_2**) are drawn in orange and red, respectively. Values were normalized as a percentage of current with reference to their control I_{ACh} at −60 mV. Each point is the average of 5 ($N = 1$) and 12 ($N = 3$) cells for 0.1 and 0.7 μM Ttc, respectively. **(C)** Kinetics of the voltage-dependent blockade of nAChRs at −60 mV. **(C_1)** I_{ACh}s were elicited by 10 μM ACh alone (control, black recordings), or together with either 0.1 μM (orange trace) or 0.7 μM Ttc (red recording) at −60 mV; during the I_{ACh} plateau, an 800 ms voltage jump to +40 mV was given (bottom trace shows the voltage protocol). Membrane leak currents (recorded in the absence of ACh) have been subtracted. **(C_2)** Zoomed in view of the areas indicated by arrows in **C_1** (immediately after the voltage jump). Kinetics of the voltage-dependent blockade of nAChRs by 0.1 μM (orange trace) and 0.7 μM Ttc (red trace) were determined by fitting the net I_{ACh} decays to exponential functions (green curves over the recordings). The small, slow I_{ACh} changes evoked by the voltage pulse when the cell was bathed solely with ACh (black recordings in **C_1**) have been subtracted. **(C_3)** Time constant values of the voltage-dependent I_{ACh} blockade kinetics elicited by 0.1 and 0.7 μM Ttc. Asterisk indicates significant differences between both values ($p < 0.05$, *t*-test).

Thus, the kinetics of the voltage-dependent blockade of I_{ACh} were accelerated with increasing Ttc concentration ($p < 0.05$, *t*-test; **Figure $2C_3$**).

Pharmacological Profile of I_{ACh} Blockade by Ttc

To better characterize the mechanisms underlying I_{ACh} inhibition by Ttc, oocytes were superfused with ACh at different concentrations (1, 3, 10, 100 μM, and 1 mM) alone, or co-applied with 0.7 μM Ttc, either directly, or after a 12 s pre-application of the same Ttc concentration (**Figure $3A_1$,A_2**, respectively). When ACh and Ttc were directly co-applied, the I_{ACh} amplitude was reduced roughly by half (as would be expected from the estimated IC_{50} of Ttc), independently of the ACh dose tested (see records in **Figures $3A_1$,B,C**). This indicates that Ttc was acting by a non-competitive mechanism of inhibition. The estimated EC_{50} values of the ACh dose-I_{ACh} amplitude curves obtained when Ttc was either co-applied, or pre- and co-applied with ACh, were similar to those observed in control curves, in which ACh was applied alone. In particular, the EC_{50} values were 37 μM for the control curve (95% CI 32–43 μM; $n = 10$–13, $N = 3$) vs. 49 μM (95% CI 42–55 μM; $n = 3$–6, $N = 2$) and 21 μM (95% CI 12–36; $n = 4$–7, $N = 2$) for the sole Ttc and ACh co-application, and the Ttc pre- and co-application, respectively ($p > 0.05$). The I_{ACh} blockade elicited by pre- and co-application of Ttc was also independent of the ACh dose (56–75% at different concentrations). However, the extent of I_{ACh} inhibition was significantly greater than that observed with ACh and Ttc co-application alone (48–55%, $p < 0.05$ ANOVA; **Figure 3C**), unless at very low ACh concentrations (3 μM). Since the probability of unliganded nAChRs being open is less than one in a million (Nayak et al., 2012), it turns out that the increased nAChR blockade by Ttc pre-application, before its co-application with ACh, is due to Ttc binding to resting (closed) nAChRs. Consequently, Ttc pre-application would block nAChRs before they can be gated by the agonist.

Differential Effects of Ttc on I_{ACh} Depending on Membrane Potential and Application Time

As mentioned above, nAChR inhibition by Ttc at relatively high concentrations (IC_{50} or above) involved both open- and closed-channel blockade. To better understand the effects of Ttc on nAChRs at these concentrations, oocytes were clamped at two different potentials (−60 or +40 mV), and I_{ACh}s were elicited by 32 s superfusion of 10 μM ACh either alone (**Figures $4A_1$-A_6**, black recordings), or with 0.7 μM Ttc (**Figures $4A_1$-A_6**, red recordings) in three different protocols as follows: (i) Ttc was co-applied with ACh (**Figures $4A_1$,A_4**); (ii) Ttc was pre-applied for 12 s before superfusion with ACh alone (**Figures $4A_2$,A_5**); and (iii) 12 s pre-application of Ttc followed by its co-application with ACh (**Figures $4A_3$,A_6**). The percentages of I_p and I_{ss} inhibition by Ttc differed, depending on the specific protocol (**Figures $4B_1$,B_2**). Thus, in oocytes clamped at −60 mV, co-application of Ttc and ACh blocked roughly half the control I_p, as expected from its estimated IC_{50} (53 ± 3%, $n = 20$, $N = 9$; **Figure $4B_1$**). However, the percentage of I_{ss}inhibition increased to 74 ± 3% (same cells; $p < 0.05$, paired *t*-test; **Figure $4B_1$**), mainly because of the acceleration of I_{ACh} decay (compare black and red recordings of **Figure $4A_1$**). When Ttc was solely pre-applied, before superfusion with ACh alone, the percentage of I_p inhibition was significantly less (36 ± 2%; $n = 12$, $N = 4$; $p < 0.05$, ANOVA; **Figure $4B_2$**) than when Ttc and ACh were co-applied. No significant differences were noted between the percentages of I_p and I_{ss}inhibition when Ttc was solely pre-applied (**Figure $4B_1$**), indicating a very slow recovery from this blockade. In contrast, Ttc pre-application, followed by its co-application with ACh significantly increased the percentage of I_p inhibition, as compared with their sole co-application (67 ± 2% vs. 53 ± 3%; $n = 15$, $N = 5$; $p < 0.05$, ANOVA and Bonferroni *t*-test; **Figure $4B_1$**). Furthermore, the I_{ss} blockade (79 ± 2%) was significantly greater than the I_p inhibition ($p < 0.05$, paired *t*-test), indicating that I_{ACh} decay was accelerated when Ttc was pre-applied, and later co-applied with ACh. Indeed, the I_{ACh} decay time constants (see below) observed when Ttc was co-applied with ACh alone, and when Ttc was pre-applied and then co-applied with ACh were similar (compare **Figure $4A_1$** and **Figure $4A_3$**). It is also interesting that the percentage of I_p remnant when Ttc was first pre-applied, and then co-applied with ACh (33%) was very close to the expected value if Ttc binding sites with sole Ttc pre-application, and Ttc and ACh co-application (64 and 47% of control I_p, respectively) were independent (30%). Thus, interactions of Ttc with resting and open nAChRs agree with an allotopic model, as we previously observed for DMA and DEA interactions on nAChRs (Alberola-Die et al., 2016b).

When the membrane potential was held at +40 mV, the extent of I_{ACh} blockade by 0.7 μM Ttc was smaller than that at −60 mV in any of the three above-mentioned protocols (**Figure $4A_4$-A_6**). Nevertheless, as observed at −60 mV,

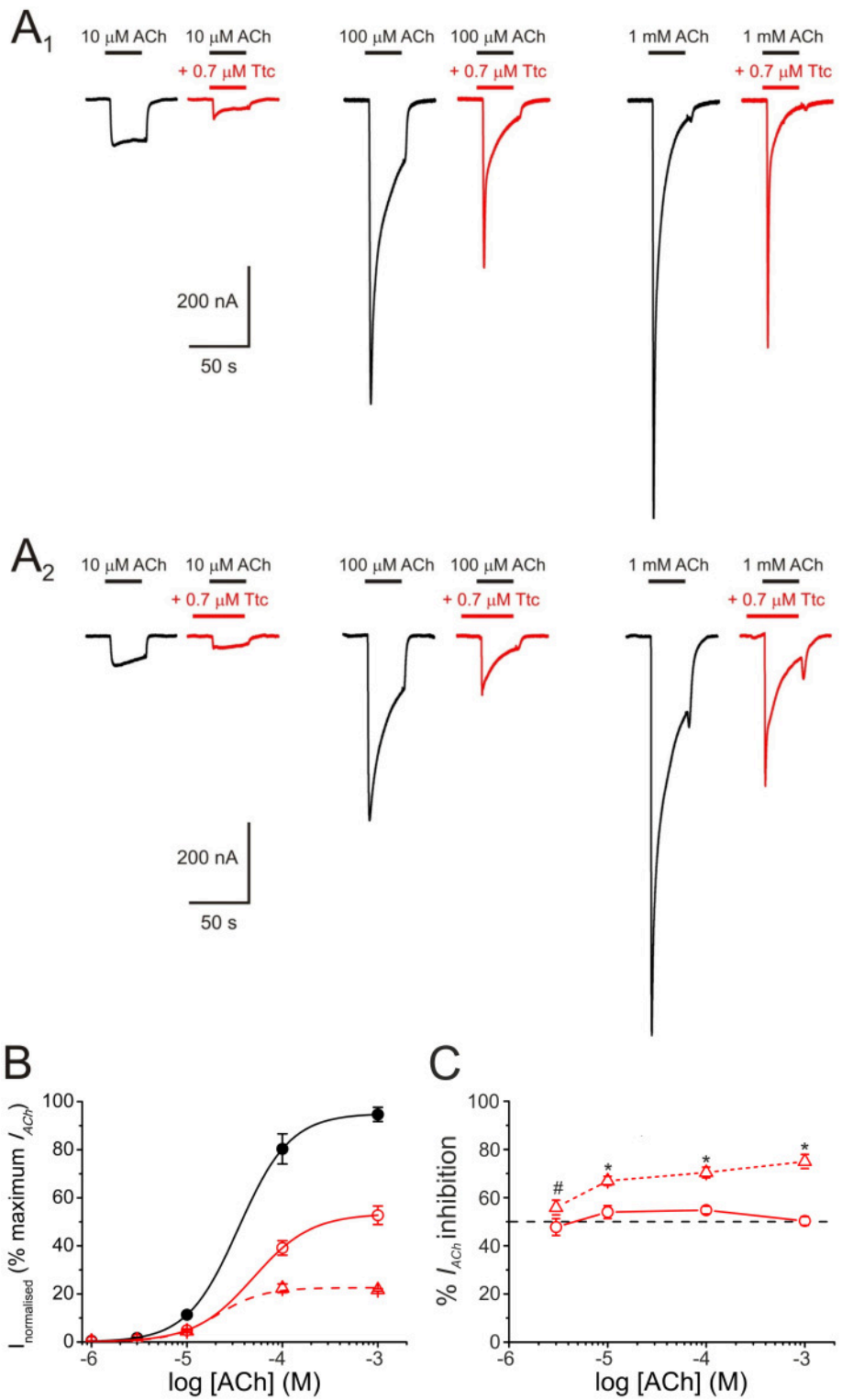

FIGURE 3 | Pharmacological profile of nicotinic acetylcholine receptor (nAChR) blockade by tetracaine (Ttc). **(A)** I_{ACh}s evoked by different ACh concentrations (10, 100 μM, and 1 mM) either alone (**A_1**,**A_2**, black recordings), co-applied with 0.7 μM Ttc (**A_1**, red recordings), or co-applied with 0.7 μM Ttc, after Ttc pre-application for 12 s at the same concentration (**A_2**, red recordings). **(B)** Averaged ACh concentration-I_{ACh}amplitude relationship. I_{ACh}s were evoked by different ACh concentrations alone (filled black circles; $n = 10$–13, $N = 3$), or co-applied with 0.7 μM Ttc, either directly (open circles; $n = 3$–6, $N = 2$), or subsequent to its pre-application (open triangles; $n = 4$–7, $N = 2$). Data were normalized to the maximal I_{ACh} elicited by ACh alone and fitted to the Hill equation (solid and dashed lines). **(C)** Percentage of

(Continued)

FIGURE 3 | I_{ACh} inhibition when different ACh concentrations were directly co-applied with 0.7 μM Ttc (circles and solid line; $n = 9$–33, $N = 4$–13), or after pre-application of the same Ttc concentration for 12 s (triangles and dashed line; $n = 11$–21, $N = 2$–6). Asterisks indicate significant differences in the percentage of I_{ACh} inhibition between ACh-Ttc co-application alone, and pre- and co-application of Ttc at each ACh concentration ($p < 0.05$, *t*-test). ACh concentration effected no significant changes in the extent of inhibition by Ttc, either when Ttc and ACh were directly co-applied, or when this co-application was preceded by Ttc pre-application ($p > 0.05$, ANOVA; except at 3 μM ACh, indicated by the pound sign. However, I_{ACh}s at such low ACh concentration are too small for accurate determination of the percentage of inhibition).

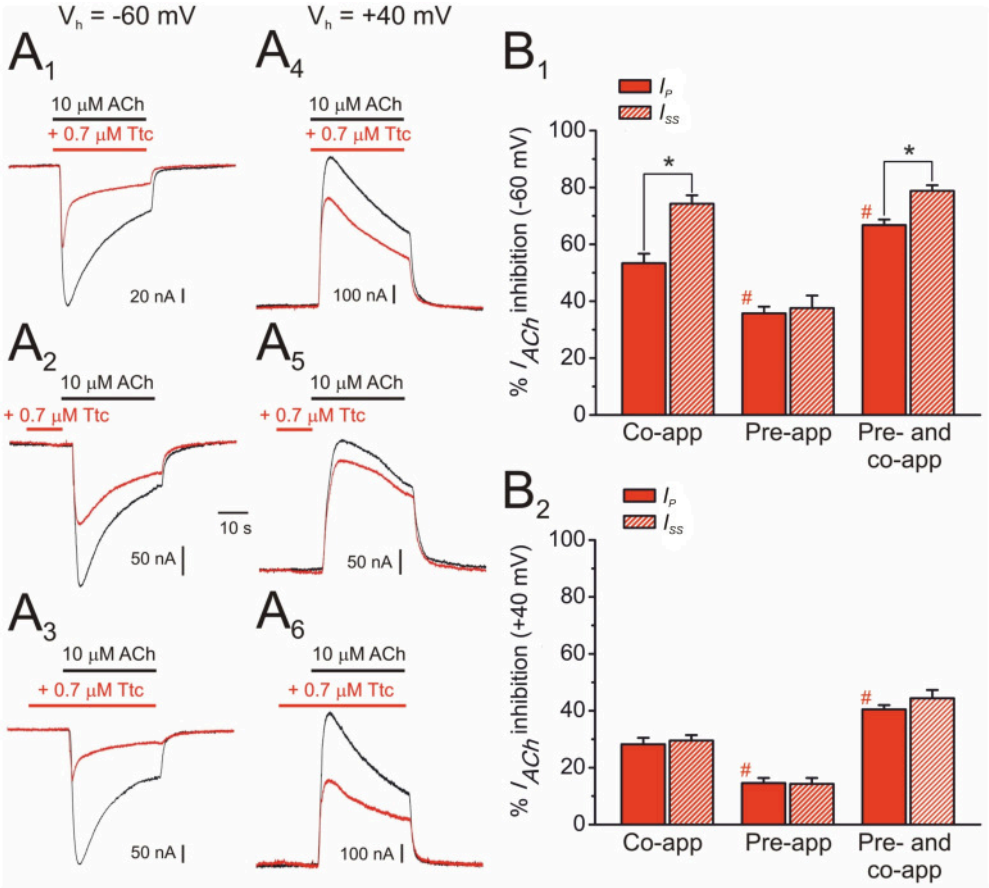

FIGURE 4 | Effect of tetracaine (Ttc) application timing and holding potential on nicotinic acetylcholine receptor (nAChR) blockade. **(A)** I_{ACh}s elicited at −60 mV **(A_1,A_2,A_3)** and at +40 mV **(A_4,A_5,A_6)** by co-application of 10 μM ACh and 0.7 μM Ttc (Co-app; **A_1,A_4**), sole Ttc pre-application before superfusion of the agonist (Pre-app; **A_2,A_5**), or Ttc pre-application followed by its co-application with ACh (Pre- and co-app; **A_3,A_6**). **(B)** Column graphs showing the percentages of I_{ACh} inhibition by Ttc at −60 mV **(B_1)** and +40 mV **(B_2)** at the I_p (red filled columns) and the I_{ss} (red striped columns), when Ttc was applied as indicated in **(A)**. Asterisks indicate significant differences between I_{ACh} inhibition by Ttc at I_p and I_{ss} ($p < 0.05$, paired *t*-test). Pound signs indicate significant differences of I_p inhibition among Ttc application-timing protocols, as compared with the values for ACh and Ttc co-application ($p < 0.05$, ANOVA and Bonferroni *t*-test). Note that I_{ACh} decay was only accelerated (i.e., significant differences observed between I_p and I_{ss} inhibition) when Ttc was either co-applied with ACh, or pre-applied and later co-applied with ACh, at −60 mV. Each column represents the average obtained from 12 to 20 oocytes ($N = 4$–9) for **(B_1)**, and from 6 to 11 cells ($N = 2$–3) for **(B_2)**.

the highest I_{ACh} inhibition was found with Ttc pre- and co-application, and the lowest inhibition with just Ttc pre-application (**Figure 4B$_2$**). Interestingly, at +40 mV, I_{ACh} decay was not enhanced by Ttc when it was either just co-applied with ACh or pre- and co-applied, in contrast to its effects observed at −60 mV. Therefore, at positive potentials the percentages of I_p and I_{ss} inhibition were similar in all tested protocols (**Figure 4B$_2$**).

In addition, we tested the effects of a 12 s pulse of 0.7 μM Ttc, applied during the I_{ss} elicited by a 40 s pulse of 10 μM ACh (**Figure 5A**). This co-application of ACh and Ttc evoked a fast and large inhibition of I_{ss} (I_{ss} reduced by 75 ± 2%; $n = 13$, $N = 4$). Notably, the kinetics of this I_{ACh} blockade showed the same temporal course as that observed for membrane currents elicited by superfusion with a high-K^+ solution. This indicates that the timing of this I_{ss} inhibition was only limited by the

perfusion kinetics (see **Figures 5B,C**). In contrast, I_{ss} recovery after Ttc removal exhibited slower kinetics (time constants of 1.49 ± 0.09 s vs. 3.00 ± 0.23 s, for Ttc onset and recovery phases, respectively; $p < 0.05$, *t*-test), which was not limited by the solution exchange kinetics (compare with the high-K^+ solution washout; **Figure 5C**). Nevertheless, the kinetics of I_{ACh} recovery when Ttc blocked open nAChRs was much faster than that after the blockade of closed nAChRs (see **Figure 4A$_2$**).

Ttc Enhancement of nAChR Desensitization

At concentrations of 0.5 μM or higher, Ttc accelerated I_{ACh} decay (see **Figure 1**). This acceleration might have originated from one of the following two mechanisms (or a combination of both): (i) a slow blocking effect of Ttc on nAChRs, which would boost I_{ACh} decline after its peak; (ii) an enhancement of nAChR desensitization. To discriminate between both possibilities, we assessed the effect of 0.7 μM Ttc on the I_{ACh} decay elicited by two different concentrations of ACh (10 and 100 μM), because desensitization is markedly dependent on agonist concentration. As previously reported, I_{ACh} decay followed a two-exponential function (see **Figures 6A$_1$,A$_2$**), although the slower component was too slow for accurate analysis using this experimental approach (Morales and Sumikawa, 1992). Thus, considering only the time constant (τ) of the fast component of I_{ACh} decay, it is clear that I_{ACh} declined at a slower rate at 10 μM ACh (**Figure 6A$_1$**; τ_{Ctr} = 15.6 ± 2.1 s, $n = 12$, $N = 6$) than at 100 μM ACh (**Figure 6A$_2$**; τ_{Ctr} = 5.9 ± 0.7 s, $n = 18$, $N = 6$; $p < 0.05$, *t*-test). In the presence of 0.7 μM Ttc, the I_{ACh} decay showed a different trend in acceleration at 10 μM (τ_{Ttc} = 1.0 ± 0.1 s) and at 100 μM ACh (τ_{Ttc} = 0.6. ± 0.1 s; $p < 0.05$, *t*-test; **Figures 6A$_1$,A$_2$**). Thus, a constant Ttc dose had a more potent effect on accelerating I_{ACh} decay when a higher concentration of ACh was used. This finding rules out the notion that the enhancement of I_{ACh} decay is merely due to a delayed nAChR blockade, mediated by slow Ttc binding. Therefore, the maximum percentage of change in I_{ACh} decay elicited by 0.7 μM Ttc was achieved earlier, when it was co-applied with 100 μM ACh (2.6 s) than with 10 μM ACh (4.2 s; **Figure 6B**, arrows). These results strongly suggest that Ttc enhances nAChR desensitization.

Co-application of 10 μM ACh with different concentrations of Ttc (0.01–2 μM) also highlights the fact that Ttc enhances nAChR desensitization at concentrations close to, or above its IC_{50}. As shown in **Figure 7**, low Ttc concentrations (0.01–0.1 μM) elicited a significant I_{ACh} blockade (up to 30%; **Figures 7A$_1$,C**), but did not modify I_{ACh} decay (**Figures 7A$_2$,B**). In contrast, ACh co-applied with 0.7–2 μM Ttc significantly increased both the extent of nAChR blockade (**Figures 7A$_3$,A$_5$,C**) and the rate of I_{ACh} decay (**Figures 7A$_4$,A$_6$,B**). The lack of an acceleration of I_{ACh} decay by low Ttc concentrations, which nonetheless reduced I_{ACh} amplitude, presents evidence against the hypothesis of a slow nAChR blockade by Ttc being responsible for a boost in I_{ACh} decay, and supports the theory that Ttc indeed enhances nAChR desensitization.

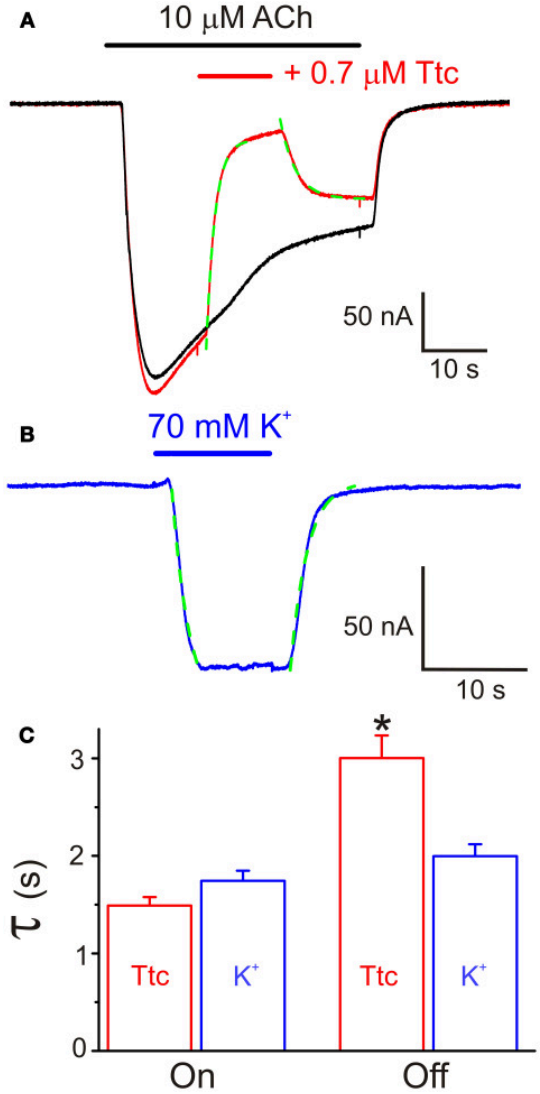

FIGURE 5 | Effect of tetracaine (Ttc) application while nicotinic acetylcholine receptors (nAChRs) were activated by 10 μM acetylcholine (ACh). **(A)** Two superimposed I_{ACh}s elicited by 40 s pulses of ACh. The red recording shows the fast inhibitory effect of 0.7 μM Ttc, superfused when indicated by the red horizontal bar. The kinetics of I_{ACh} inhibition followed an exponential function (green trace) with a time constant similar to those found for membrane currents evoked by superfusion of a high-K^+ (70 mM) solution (blue recording in **B**). Onset and decay of the K^+ current were fitted to exponential functions (discontinuous green line). **(C)** Time constant values of the exponential functions fitted to the onset (On) and recovery (Off) of I_{ACh} blockade by Ttc and K^+ currents. Note that the rate of I_{ACh} inhibition is conditioned by the solution exchange kinetics, but I_{ACh} recovery, after Ttc removal, exhibited slower kinetics. Asterisk indicates significant differences ($n = 13$, $p < 0.05$, ANOVA test).

Further evidence indicating that Ttc promotes faster nAChR desensitization arise from computation of the ratios of I_{ss} vs. I_p amplitudes, when co-applying 10 μM ACh with different

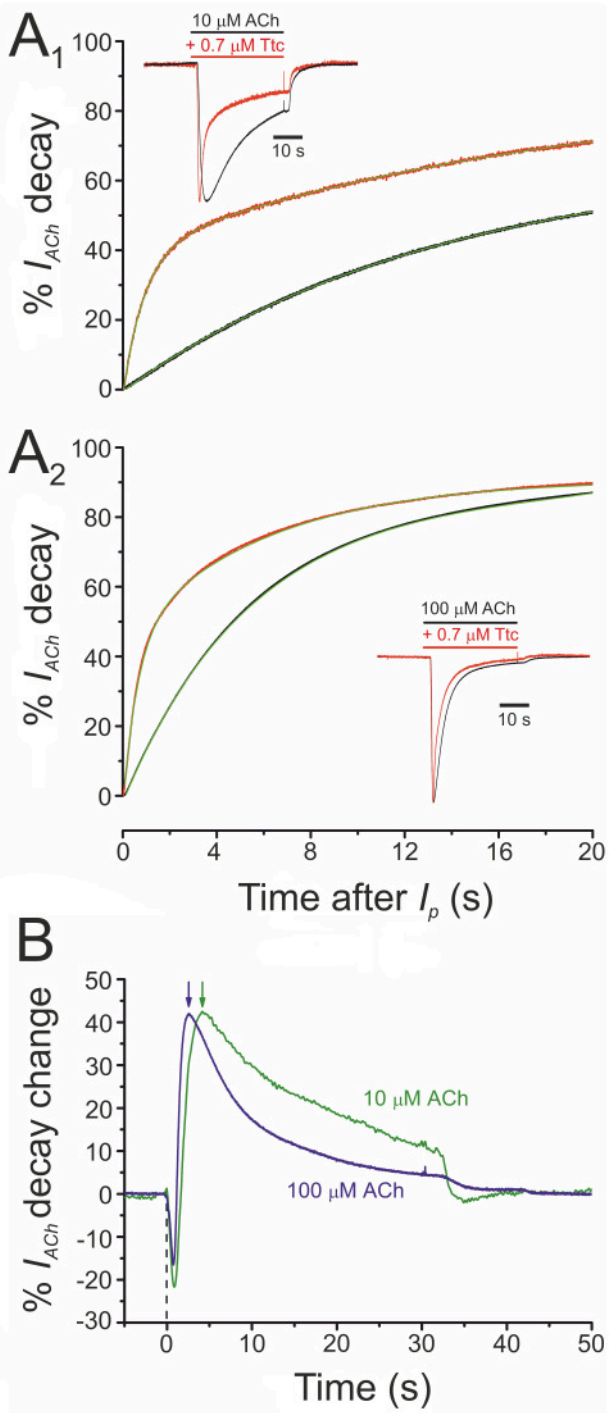

FIGURE 6 | Acceleration of I_{ACh} decay by tetracaine (Ttc) is dependent on the concentration of acetylcholine (ACh). **(A)** Plot of averaged I_{ACh} decay (expressed in percentages) elicited by 10 μM ACh (**A$_1$**; $n = 12$, $N = 6$) or 100 μM ACh (**A$_2$**; $n = 18$, $N = 6$), either alone (black recordings) or co-applied with 0.7 μM Ttc (red traces). Green lines over the averaged recordings represent two-exponential functions fitted to the I_{ACh} decay. Insets are representative recordings of I_{ACh}s elicited by 10 μM ACh **(A$_1$)** or 100 μM ACh **(A$_2$)**, either alone (black recordings), or co-applied with 0.7 μM Ttc (red traces). The I_p amplitudes in the presence of Ttc have been normalized to their

(Continued)

FIGURE 6 | control values for easier comparison of decay kinetics. **(B)** Averaged percentages of change in I_{ACh} decay elicited by 0.7 μM Ttc, computed as the difference between I_{ACh}s obtained in the absence and presence of Ttc, for currents evoked by 10 μM ACh (green line; $n = 12$; $N = 6$) or 100 μM ACh (blue line; $n = 18$, $N = 6$). Notice the earlier maximum decay acceleration (arrows) when I_{ACh} was evoked by 100 μM ACh. Zero time corresponds to the beginning of Ttc-ACh co-application and the downward deflections are due to the earlier I_p in the presence of Ttc (see inset of **A$_1$**).

concentrations of Ttc, as proposed by Sobolevsky et al. (1999) (see Equation 2 in section Materials and Methods and **Figure 8**). At low concentrations of Ttc (lower than 0.5 μM), the quotient of the I_{ss} to I_p ratio in the presence of Ttc (I_{ss_Ttc}/I_{p_Ttc}) over the I_{ss} to I_p ratio in the presence of ACh alone (I_{ss_Ctr}/I_{p_Ctr}) was close to 1. However, at higher Ttc concentrations (0.5 μM or above), this quotient was significantly smaller than 1 ($p < 0.05$; one-sample t-test), and interestingly, was reduced in a dose-dependent manner, as the extent of I_{ss} inhibition by Ttc increased (**Figure 8B**). Therefore, the plot in **Figure 8B** illustrates that low Ttc concentrations elicit nAChR blockade without affecting I_{ACh} decay, whereas Ttc concentrations over 0.5 μM evoke both (i) I_{ACh} reduction by nAChR blockade; and (ii) acceleration of I_{ACh} decay by enhancement of nAChR desensitization.

On the other hand, the kinetics of I_{ACh} tails (deactivation) differed when ACh was withdrawn, but Ttc remained in the ANR. In these experiments, 100 μM ACh, which evokes considerable nAChR desensitization, was co-applied with either 0.1 or 0.7 μM Ttc for 32 s, and ACh was then washed out, while keeping the cell superfused with Ttc for an additional 12 s. As previously shown, the effects of Ttc on I_{ACh} are concentration-dependent. Thus, 0.1 μM Ttc elicited both a small I_{ACh} reduction, and a slight, but significant, enhancement of I_{ACh} decay, mainly of the fast desensitization component (**Figures 9A$_1$,A$_2$**). Thus, the ratio of I_{ACh} decay time constant values obtained in the presence of 0.1 μM Ttc vs. ACh alone was significantly smaller than 1 (0.69 ± 0.07; $n = 12$, $N = 6$; $p < 0.05$, one-sample t-test). Notably, co-application of 10 μM ACh together with 0.1 μM Ttc did not modify I_{ACh} decay (**Figures 7A$_2$,B**), whereas the same concentration of Ttc co-applied with 100 μM ACh significantly accelerated I_{ACh} decay (**Figure 9A$_2$**). When 100 μM ACh was co-applied with 0.7 μM Ttc, nAChR blockade was increased and I_{ACh} decay was accelerated (**Figures 9A$_1$,A$_2$**). The ratio of I_{ACh} decay time constant values obtained in the presence of 0.7 μM Ttc and ACh alone was 0.23 ± 0.08 ($n = 13$, $N = 8$). This indicates that at this Ttc dose, the I_{ACh} decayed significantly faster than in the presence of 0.1 μM Ttc ($p < 0.05$, t-test). Moreover, I_{ACh} deactivation after ACh withdrawal, followed a single exponential time course, the kinetics of which was affected by keeping Ttc in the ANR (**Figures 9A$_3$,A$_4$**). Deactivation of control I_{ACh}s, elicited by ACh alone, followed an exponential function with a time course that was limited by the solution exchange kinetics (time constant of 1.4 ± 0.1 s, $n = 25$; see **Figure 5**); thus, we would refer to these values as apparent deactivation time constants ($\tau_{\text{apparent}-\text{deactivation}}$). The presence

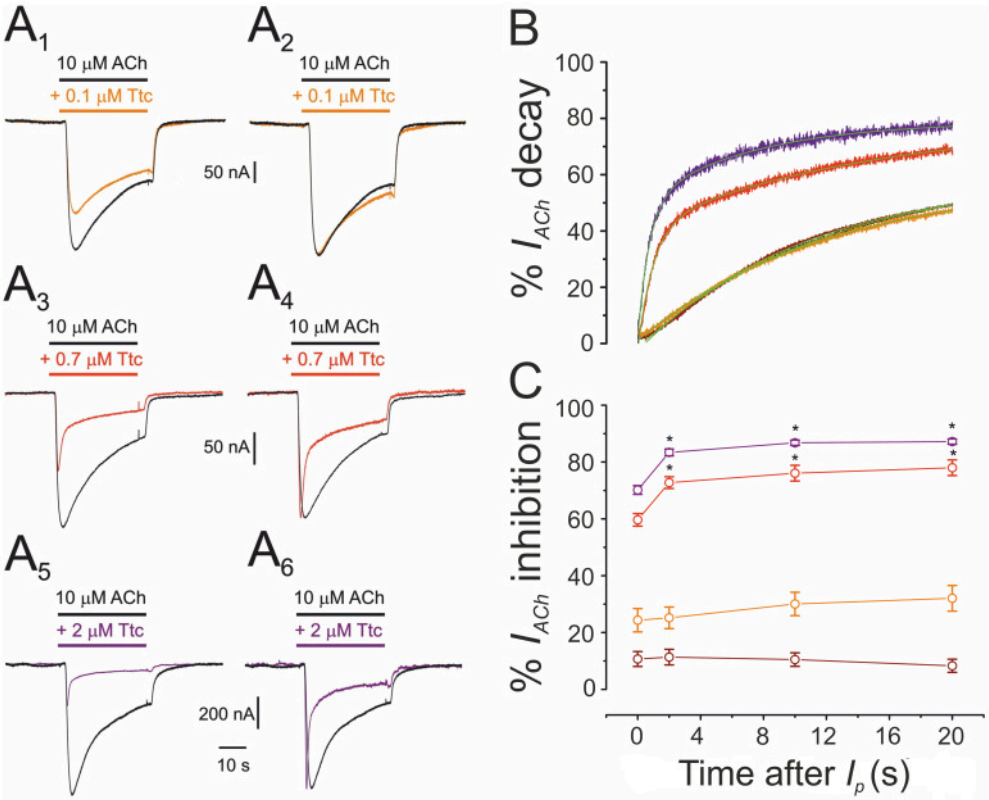

FIGURE 7 | Acceleration of the decay of currents elicited by ACh (I_{ACh}) is dependent on the concentration of tetracaine (Ttc). **(A)** Representative I_{ACh}s elicited by 10 μM ACh, either alone (black; **A_1-A_6**), or co-applied with 0.1 μM (orange; **A_1**), 0.7 μM (red; **A_3**), or 2 μM Ttc (purple; **A_5**). The same I_{ACh}s are in the right-hand **(A_2,A_4,A_6)**, but their peak amplitudes were normalized to show more effectively the differences on I_{ACh} decay. **(B)** Normalized and averaged I_{ACh} decay elicited by 10 μM ACh, either alone (black trace; $n = 43$, $N = 12$), or plus 0.01 μM (brown trace; $n = 12$, $N = 4$); 0.1 μM (orange trace; $n = 9$, $N = 3$); 0.7 μM (red trace; $n = 12$, $N = 6$); or 2 μM Ttc (purple trace; $n = 10$, $N = 4$). Each averaged I_{ACh} decay was fitted by a two-exponential function (green lines overlapping each recording). Note that with Ttc concentrations of up to 0.1 μM, the I_{ACh} decay overlaps the control. **(C)** Percentages of I_{ACh} inhibition by 0.01, 0.1, 0.7, and 2 μM Ttc (same cells and color codes as in **B**) at different times after I_p. Low Ttc concentrations blocked nAChRs, but they did not modify I_{ACh} decay. In addition, note that the time-dependent increase in the percentage of I_{ACh} inhibition was already established 2 s after I_p. For each Ttc concentration, asterisks indicate significant differences among the percentages of I_{ACh} inhibition at different times, as compared with their respective I_p ($p < 0.05$, ANOVA, Bonferroni *t*-test).

of Ttc decelerated I_{ACh} deactivation in a dose-dependent manner ($\tau_{apparent-deactivation}$ of 1.9 ± 0.3 and 2.9 ± 0.3 s for I_{ACh}s in the presence of 0.1 and 0.7 μM Ttc, respectively; same cells as above; **Figures 9A_3,A_4,B**), as ACh washout kinetics remained constant. Deceleration of I_{ACh} deactivation would be expected if Ttc enhances nAChR desensitization, as has been previously reported for $GABA_A$Rs (Jones and Westbrook, 1995). Accordingly, a linear correlation exists between the extent of desensitization (see Equation 2 in section Materials and Methods) and the apparent deactivation time constant values in the presence or absence of Ttc (**Figure 9B**).

Virtual Docking Assays

The interactions between Ttc and the nAChR were explored by using the full structure of *Torpedo* nAChRs as a template in both the open and closed conformations (Alberola-Die et al., 2016a,b). For each conformation we carried out 800 runs to assess Ttc-nAChR interactions. We found 279 clusters of interaction sites differing by less than 5 Å of the root-mean-square-deviation for the nAChR in the open state and 257 in the closed state. As shown in **Figure S3** (open state) and **Figure S4** (closed state), these clusters were located at the ECD (87 and 89% for open and closed states, respectively) and at the TMD (13 and 11% for open and closed states, respectively). No clusters were found at the intracellular domain (ICD). Most nAChR-Ttc interactions at the ECD involved two subunits (53 and 57% for open and closed states, respectively), mainly α_1-γ, α_2-δ, close to the orthosteric binding site, and α_1-β for both the open and closed states (**Figures S3Cc_1, S4Cc_1**). In contrast, TMD clusters were involved in simultaneous binding to residues of 3–5 subunits deep within the channel pore (**Figures S3Cc_2, S4Cc_2**). In addition, there were TMD clusters located close to the ECD-TMD interface, at intra- or inter-subunit crevices, comprising 1 or 2 subunits, respectively (**Figures S3Cc_3,c_4, S4Cc_3,c_4**). Notably, Ttc was bound to roughly the same nAChR residues within the channel pore in both open and closed states (see **Table 1**). Conversely, less overlapping was observed with respect to Ttc binding to residues at the ECD and inter- and intra-subunit crevices of the TMD. Thus, only

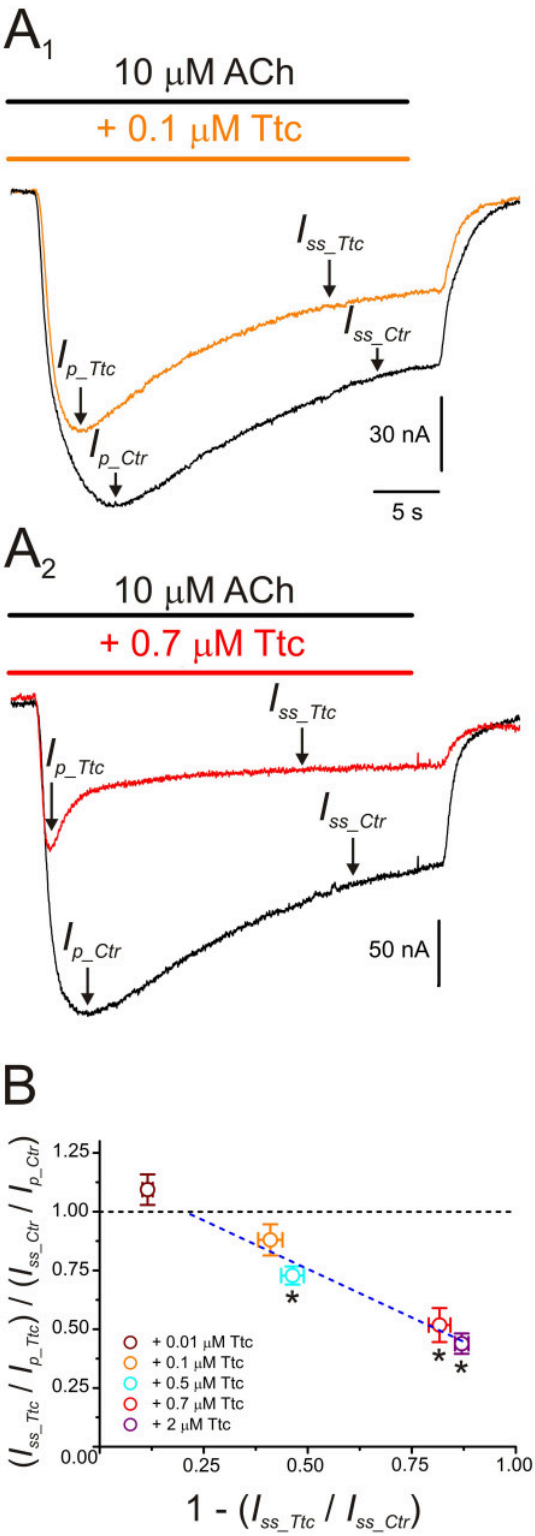

FIGURE 8 | I_{ACh} desensitization increases with increasing tetracaine (Ttc) concentration. **(A)** I_{ACh}s evoked by 10 μM ACh, either alone (black; **A_1**,**A_2**) or co-applied with 0.1 μM (orange recording; **A_1**), or 0.7 μM Ttc (red trace; **A_2**). I_p and I_{ss} values are indicated by arrows in the I_{ACh}s elicited solely by ACh (I_{p_Ctr} and I_{ss_Ctr}), or together with Ttc (I_{p_Ttc} and I_{ss_Ttc}). Note that I_{p_Ttc} *(Continued)*

FIGURE 8 | was reached earlier than I_{p_Ctr}. **(B)** Relationship between changes in I_{ACh} desensitization (see Equation 2) and extent of I_{ss} inhibition evoked by different concentrations of Ttc (0.01–2 μM). The black discontinuous line is a reference indicating no change in desensitization and the blue line is the best linear fit to values falling below the reference line (0.1–2 μM Ttc). Each point represents the average obtained from 7 to 19 oocytes ($N = 2$–9), except for 0.5 μM Ttc, in which $n = 3$ and $N = 1$. Asterisks indicate significant differences from control desensitization ($p < 0.05$, one-sample *t*-test).

22 out of 47 (46.8%) residues that were bound to Ttc at the ECD in the closed state were also bound to this LA in the open state (**Table 1**). A similar percentage of coincidence was found when considering intra- and inter-subunit residues of the TMD, specifically 16 out of 26 (61.5%) and 14 out of 33 (42.4%), respectively (**Table 1**).

Given the strong effect of Ttc on I_{ACh} decay elicited by the enhancement of nAChR desensitization, and the presence of this effect only at negative potentials (see **Figure 4**), it is logical to consider that Ttc increases desensitization through its binding within the channel pore. To assess this hypothesis, we performed additional docking assays focused just at the channel pore when it was in the open conformation. Further, 150 runs were performed to assess Ttc-nAChR channel pore interactions and docking developed at the same residues located at the middle of the channel pore, in a similar manner to those reported above, using the whole nAChR structure (**Figure S3Cc$_2$**, and **Figure 10Aa$_1$**). In an attempt to explore further Ttc-nAChR interactions in the channel, we blocked Ttc binding at the residues indicated above. Additional runs carried out under the specified conditions showed that Ttc also binds, although with a lower affinity, to residues of α_1, α_2 (E262 and L263), and γ subunits (N224, L267, Q270, K271, and E274), located at the channel pore, close to the extracellular side (**Figures 10Aa$_2$,B**; **Table 1**). Interestingly, when this approach was repeated using the nAChR in the closed conformation, we found that Ttc was bound to coincident sites within the channel pore, despite the fact that the sole pre-application of Ttc did not affect the rate of I_{ACh} decay (**Figure 4A$_2$**).

Table 2 reflects the theoretical binding energy and K_d values (Equation 4) of Ttc docking solutions at the three main nAChR binding sites both in the resting and open states: *site-1*, the ECD; *site-2*, the outer mouth of the pore; and *site-3*, located deeper within the channel pore (see image of **Table 2**). In the resting state, the binding energy of site 2, which corresponds to the low-affinity site, was lower than those of either sites 1 (ECD) or 3 (the high-affinity site within the pore). Similarly, in the open state, the Ttc binding energy of site 2 was significantly lower than those observed for sites 1 and 3 ($p < 0.05$, *t*-test). In contrast, the ECD sites presented similar K_d values, both in the open and resting states, and they were comparable to those of site 3 in the closed state. Additional binding energy data with details of interfaces and locations are depicted in **Table S1**.

When the present manuscript was under review, Newcombe et al. (2018) published a refined structural model of the nicotinic

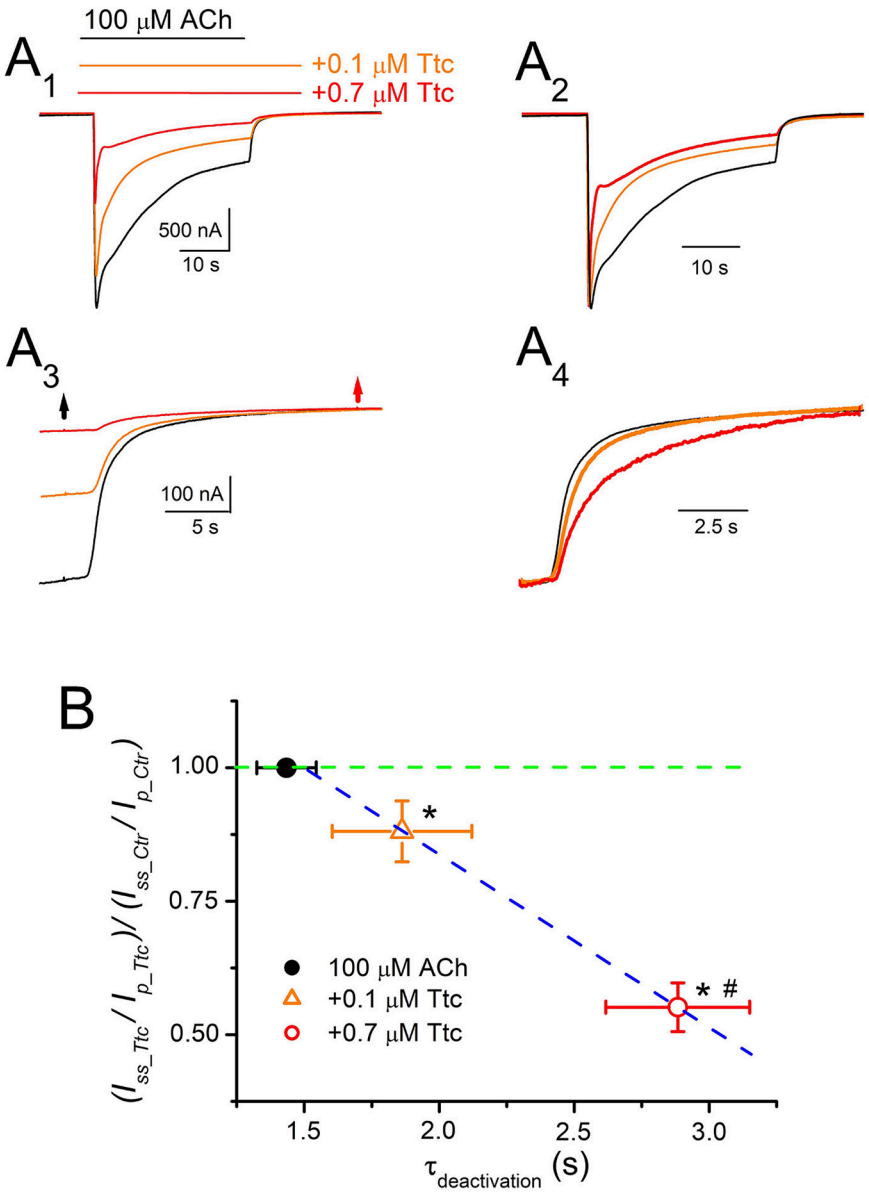

FIGURE 9 | Deactivation kinetics of currents elicited by ACh (I_{ACh}) are dependent on the concentration of tetracaine (Ttc). **(A)** Representative I_{ACh}s elicited by 100 μM ACh, either alone (black recording), or together with 0.1 μM (orange) or 0.7 μM (red) Ttc **(A_1)**. Superfusion of Ttc lasted 12 s after ACh washout. These recordings were normalized to the same I_p **(A_2)** to show changes in desensitization more effectively. **(A_3)** Deactivation of I_{ACh}s shown in **(A_1)**. The black arrow indicates ACh washout and the red arrow indicates Ttc removal. **(A_4)** I_{ACh} deactivations shown in **(A_3)** were scaled to the same amplitude to better compare their time course. **(B)** Relationship between desensitization changes (Equation 2) and the apparent deactivation time constant ($\tau_{apparent-deactivation}$) elicited by 0.1 μM (orange triangle) and 0.7 μM (red circle) Ttc. The black filled symbol corresponds to the $\tau_{apparent-deactivation}$ of I_{ACh}s elicited by ACh alone, which is rate limited by the solution exchange kinetics. The green discontinuous line indicates the control desensitization ratio. Note the higher desensitization rate elicited by Ttc (values lower than 1 in the ordinate), and the slower deactivation rate (higher $\tau_{apparent-deactivation}$ values in the abscissa) following a linear relationship (blue discontinuous line). Each point represents the average of 12–25 oocytes from eight donors. Asterisks indicate significant differences in desensitization and deactivation ($p < 0.05$, *t*-test), with respect to control values and the pound means differences in both parameters depending on the Ttc concentration used ($p < 0.05$, *t*-test).

α_7 subunit. This model corrects a previously identified error in the TMD alignment of *Torpedo* subunits, which mainly involves a shift of one helix turn at the base of the M1-M2 helices. As a refined model for the different subunits forming the muscle-type nAChR is not available, we used the structure of homomeric α_7 nAChRs, in both the open and closed states, to assess the relevance of the M1-M2 loop and nearby M2 residues in Ttc binding. After conducting 800 docking runs in each conformation, we found no Ttc interactions on the M1-M2 loop or nearby residues of the M2 helix (see **Figure S5**). Therefore, the

TABLE 1 | Nicotinic acetylcholine receptor (nAChR) residues interacting with tetracaine (Ttc) in open and resting (closed) states.

Receptor state	Domain (location)	Interfaces	Subunits	Residues
Open	**EC**	α-γ	α_γ	W149, T150, Y151, D152, Y190, P197, Y198
			γ	R78, Y116, L118, P120
		α-δ	α_δ	W149, T150, Y151, D152, P197, Y198
			δ	S40, N55, W57
		α-β	α_γ	T106, K107, L108, L109, M117, W118, T119, P120
			β	Y149, T150, Y151, D152
	TM (M2)		$\alpha_\gamma/\alpha_\delta$	S248, L251, S252, V255, F256, E262, L263
			β	S254, L257, A258, V261, F262
			δ	C262, L265, A266, V269, F270
			γ	N224, S256, L259, A260, I263, F264, L267, Q270, K271, E274
	TM (intersubunit)	β-δ	β	F219, Y220, V222, Y223
			δ	L287, I288, G289, L292, M296
		α-γ	α_δ	F214, N217, V218, I220, P221, L224
			γ	T262, L265, F266, A269, P273
	TM (intrasubunit)		$\alpha_\gamma/\alpha_\delta$	I264, L273, Y277, M278, F280, T281, F284
			β	K269, V270, S274, P278, I279, I280, I281, Y283
			δ	K224, Y228, F232, I233, L278, L287, Y291, F294, I295
			γ	L219, I222, I225, I226, Y285, F288, V289, T468
Resting	**EC**	α-γ	α_γ	V91, L92, Y93, A96, I148, **W149, T150, D152, Y198**
			γ	W54, **R78,** L108, **Y116, L118**
		α-δ	α_δ	V91, L92, Y93, N95, A96, I148, **W149, Y198**
			δ	**S40,** N41, **N55, W57,** V104, P123, I125
		α-β	α_γ	R55, **T106, K107, L108, L109, W118, T119, P120,** P121
			β	V91, L92, N96, G98, S99, F100, **Y149, T150, Y151**
	TM (M2)		$\alpha_\gamma/\alpha_\delta$	**S248, L251, S252, V255, F256**, **E262**
			β	**S254, L257, A258, V261, F262**
			δ	**C262, L265, A266, V269, F270**
			γ	**N224**, **S256, L259, A260, I263, F264**, **K271**
	TM (intersubunit)	β-δ	β	P217, L218, **F219, Y220,** I221, **V222, Y223**
			δ	L278, P279, A282, L283, V285, P286, **L287, L292**
		α-γ	α_δ	**N217, I220, P221, L224,** F225, L228, L253, F256, I260
			γ	**T262, L265, F266,** I268, **A269,** M290, S293, L294, V297
	TM (intrasubunit)		$\alpha_\gamma/\alpha_\delta$	**L273, Y277, M278, F280, T281, F284**
			β	**V270, S274,** V277, **P278, I279, I280, I281, Y283**
			δ	**Y291, F294,** L298, G301, V302, N305
			γ	I268, **F288, V289,** V292, S293, I296

Main nAChR residues at extracellular (EC) or transmembrane (TM) domains, where Ttc binds when the receptor is in the open or the resting state. Red labeled residues are located at a shallow depth within the channel pore and seem to be involved in enhancement of the desensitizing effects of Ttc. Coincident interacting residues in both nAChR configurations are indicated in bold font in the resting state.

M1-M2 loop and nearby residues do not appear to be relevant targets of Ttc, at least in the homomeric nAChR. In addition, the inaccuracies of the original *Torpedo* structural model do not seem to substantially affect the docking results presented above.

DISCUSSION

This work confirms that Ttc is a powerful blocker of muscle-type nAChRs and deepens our understanding of the modulatory mechanisms of LAs associated with nAChR function. Along with other LAs that possess tertiary amine groups, such as lidocaine, Ttc shares some similar effects on nAChRs. However, there are also significant differences among their effects. For instance, the potency of Ttc as a nAChR blocker (IC_{50} of 0.3 and 0.7 μM, for the I_{ss} and I_p, respectively) is comparable to that of d-tubocurarine, and markedly higher than those of lidocaine (11–73 μM) (Gentry and Lukas, 2001; Alberola-Die et al., 2011) or procaine (25–230 μM) (Adams, 1977; Koblin and Lester, 1979; Gentry and Lukas, 2001; Wang et al., 2010).

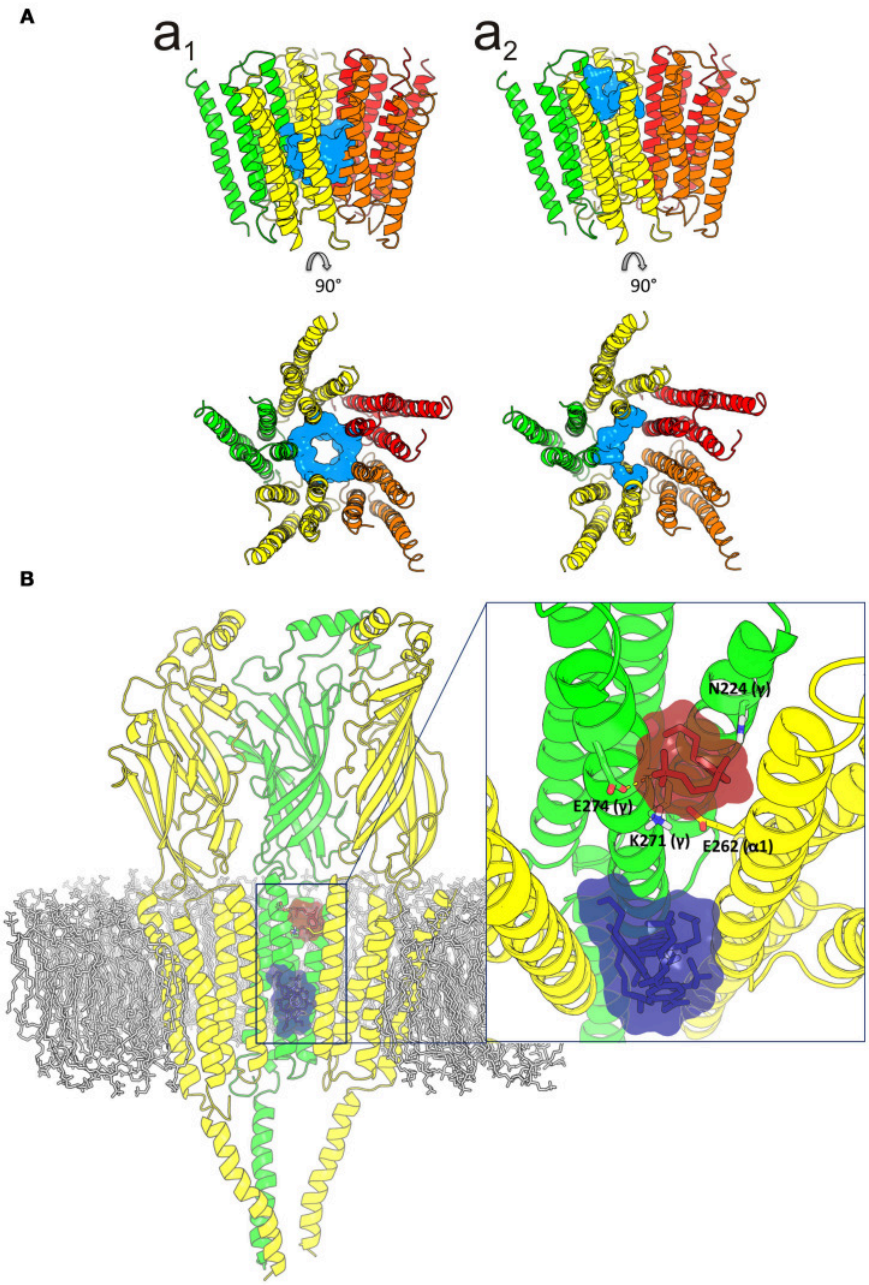

FIGURE 10 | Idealization of two putative tetracaine (Ttc) binding sites within the channel pore. **(A)** Lateral (upper) and top (lower) views of the transmembrane domain (TMD), in the open nicotinic acetylcholine receptor (nAChR), showing Ttc (highlighted in cyan) bound at the higher affinity (at the middle of the pore; $\mathbf{a_1}$) and lower affinity (closer to the extracellular side; $\mathbf{a_2}$) sites. **(B)** Lateral view of the three nAChR domains (membrane bilayer in gray). The two Ttc binding loci within the channel pore are highlighted by a square. A zoomed in image of this frame, from the synaptic cleft, is shown on the right. Ttc molecules (in purple) were used to block the high-affinity site within the pore, to reveal the Ttc low-affinity binding site (Ttc interacting molecules shown in brown), which includes E262(α), N224(γ), K271(γ), and E274(γ) as key interacting residues.

Notably, the Ttc IC_{50} here reported is roughly one order of magnitude smaller than the value found for muscle-type nAChRs expressed in a human cell line (TE671/RD; 13 μM) (Gentry and Lukas, 2001) and roughly one hundredth the IC_{50} reported for mouse cells (BC3H-1; 38 μM) (Eterović et al., 1993). Nevertheless, our Ttc IC_{50} was similar to the value stated for nAChRs from the electric organ of *Torpedo californica* expressed in *Xenopus* oocytes (1 μM) (Eterović et al., 1993), but smaller

TABLE 2 | Binding energies and dissociation constants (K_d) of tetracaine (Ttc) bound to closed and open muscle-type nicotinic acetylcholine receptors (nAChRs).

Receptor state	Binding site location	Mean binding energy (kcal/mol)	(*n*)	K_d (M)
Resting	1	4.79 ± 0.54	133	3.08×10^{-4}
	2	3.67 ± 0.67*	12	2.05×10^{-3}
	3	4.75 ± 0.19	66	3.31×10^{-4}
Open	1	4.53 ± 0.66	107	4.74×10^{-4}
	2	3.48 ± 0.36*	33	2.79×10^{-3}
	3	3.94 ± 0.51#	58	1.28×10^{-3}

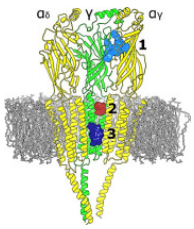

The main Ttc binding sites are denoted as (1) at the extracellular domain (ECD); (2) at the low-affinity site within the pore; and (3) at the high-affinity site within the pore. See right-hand figure for their location within the nAChR. Different binding energies of the same locations were averaged to get a single energy value, which is indicated together with its standard deviation. The K_ds were calculated using Equation 4 (see section Materials and Methods). Asterisks indicate significant differences between Ttc binding energies of site 2 and those of either sites 1 or 3, in both the open and closed conformations ($p < 0.05$, t-test); the pound sign denotes significant differences between sites 1 and 3 in the open state; n is the number of docking solutions that were averaged.

than that obtained for nAChRs from *Electrophorus electricus* electroplaques (25 μM) (Koblin and Lester, 1979). The large differences in the blocking potency of Ttc among nAChRs from the electric organ and muscle-type nAChRs expressed in diverse cells lines could be due to the different subunit conformations of these receptors; specifically, the synaptic-type (ε-like subunit) composition of the former and the extrasynaptic-type (γ-like subunit) composition of the latter. Nevertheless, whether or not muscle-type nAChRs from fetal (or denervated muscle) and adult muscles have the same sensitivity to Ttc remains to be assessed.

The main effect of Ttc on nAChRs at low concentrations, below its IC_{50}, was a voltage-dependent blockade (**Figures 2A$_1$,B$_1$**), indicating that Ttc enters the channel pore. This blockade resembles that elicited by other LAs and compounds with tertiary amine groups, such as lidocaine (Alberola-Die et al., 2011), procaine (Adams, 1977), and DEA (Alberola-Die et al., 2016a). The kinetics of the voltage-dependent blockade was assessed by stepping back the cell membrane potential from +40 mV (which ejects Ttc from its binding site within the channel) to −60 mV, while the cell was superfused with 10 μM ACh and Ttc. At 0.1 μM, Ttc most likely binds only to the high-affinity site (site 3) within the channel, and the elicited voltage-dependent blockade could be fitted by a single exponential function. Notably, at 0.7 μM Ttc (a concentration at which Ttc might bind to sites 2 and 3), the blocking kinetics also followed a single exponential function, but with a faster time constant, as would be expected with an increase in the number of blocking molecules. Therefore, these results suggest that most of the voltage-dependent blockade by Ttc is due to its binding to site 3. In accordance with these findings, the slope of the voltage-dependent blockade at negative potentials remains essentially unaltered at different concentrations of Ttc (see **Figure S2**). It should be noted that the voltage-dependent blockade of nAChRs by charged molecules is intermittent, with very fast kinetics, causing the characteristic current "flickering" (Neher and Steinbach, 1978). In contrast, it is likely that the effect on desensitization is a more long-lasting phenomenon, as it involves conformational changes. Thus, it is possible that Ttc binding to site 2 mainly promotes nAChR desensitization, leading to non-conducting desensitized nAChR, instead of a plain open-channel blockade, which is more easily reversible. At high concentrations (IC_{50} or above), Ttc also elicited a voltage-independent blockade of nAChRs (**Figures 2A$_2$,B$_2$**). This additional nAChR blockade is most likely due to the action of Ttc on nAChR residues located outside the channel pore, as it was also present at positive potentials, which should have removed most of the positively charged Ttc from the pore. Nevertheless, according to the Woodhull model (Woodhull, 1973), some I_{ACh} inhibition could be observed at positive potentials when using relatively high blocker concentrations, if the blocker binds at a shallow site within the channel pore, as Ttc does (see the mild slope of the voltage-dependent blockade of I_{ACh} in **Figure S2**). Even so, the charged cholinesterase inhibitor BW284c51, which elicits open-channel blockade of *Torpedo* nAChRs through its binding to a shallow site within the channel (delta of 0.1; i.e., very close to the extracellular side) (Olivera-Bravo et al., 2007) does not inhibit I_{ACh} at positive potentials, when tested at its IC_{50} (Olivera-Bravo et al., 2005, 2007). Moreover, the hypothesis of a single Ttc binding site cannot explain several key experimental results reported in the present study, such as: (i) the marked differences between Ttc unbinding kinetics when Ttc is just pre-applied (either at −60 or +40 mV; **Figure 4A$_2$,A$_5$**) and when it is applied during the I_{ACh} (**Figure 5**); (ii) the higher nAChR blockade evoked by 0.7 μM Ttc when it is pre-applied and then co-applied with ACh, as compared to the effect of just Ttc and ACh co-application (**Figures 4B$_1$,B$_2$**); (iii) the changes *in* I_{ACh} decay, found solely when ACh was co-applied with Ttc at concentrations close to, or above, the IC_{50} (**Figure 7B**); (iv) the slower I_{ACh} deactivation in the presence of Ttc, and its correlation with the acceleration of I_{ACh} decay (**Figure 9B**), which strongly suggests that both are due to the enhancement of nAChR desensitization; (v) the lack of acceleration in I_{ACh} decay by Ttc when holding the membrane potential at positive potentials (compare recordings **Figure 4A$_1$** and **Figure 4A$_4$**); and (vi) the different nAChR-Ttc interaction sites found in our docking assays, associated with both the ECD and TMD (see inset of **Table 2** and **Figures S3**, **S4**). All these experimental data provide strong evidence (although not irrefutable proof) that the

effects of Ttc on I_{ACh} are mediated by its binding to multiple sites in the nAChR.

As indicated above, Ttc increased its inhibitory effect when pre-applied to the cell, before its co-application with ACh (**Figure 3B,C**), suggesting a resting-channel blockade. Indeed, Ttc binding to closed nAChRs has been previously reported, either by measuring the inhibition of labeled perhydrohistrionicotoxin binding to nAChR-enriched membrane fragments (Blanchard et al., 1979; Middleton et al., 1999) or by photolabeling nAChR-rich membranes with radioactive Ttc (Gallagher and Cohen, 1999; Middleton et al., 1999). These authors found a Ttc binding affinity roughly 30-fold higher in the resting state than in the desensitized state ($IC_{50}s$ of $\approx$ 1 μM vs. 30 μM, respectively; Blanchard et al., 1979; Middleton et al., 1999), and reported that Ttc binds within the channel pore while the nAChR is in the closed state (Gallagher and Cohen, 1999). Accordingly, our docking assays on nAChRs showed that Ttc binds within the channel pore, both in the open and closed conformations (site 3 of **Table 2**; **Figures S3A,Cc$_2$**, **S4A,Cc$_2$**, respectively), and become involved with the same residues in both states (see **Table 1**). Notably, the M2 residues interacting with Ttc at the middle of the channel pore are roughly the same as those reported for Ttc interactions with resting nAChRs (Gallagher and Cohen, 1999). Although our *in silico* results do not show that M2 residues had a higher Ttc binding affinity when the nAChR was in the open state, the selective open-channel blockade elicited by low concentrations of Ttc indicate that these residues should have had the highest affinity for Ttc. Nevertheless, the docking data revealed that the Ttc binding energies of site 3 were significantly higher than those of site 2 (located at a shallower depth in the TMD; see **Table 2**) and roughly similar to those of site 1 (binding sites at the ECD). Our virtual docking assays on the resting nAChR showed that Ttc interacts mostly with residues located at the ECD (**Figure S4**). Furthermore, the functional results suggest that Ttc binds to different (independent) sites, whether the nAChR is closed or open (**Figure 4**), and this binding is dependent on the concentration of Ttc administered. In this regard, it should be pointed out that the concentration of Ttc used for the photolabeling experiments was 5 μM (Gallagher and Cohen, 1999), which is almost one order of magnitude higher than our IC_{50} value, and roughly 50-fold the concentration of Ttc that elicits selective voltage-dependent blockade of nAChRs (**Figures 2A$_1$,B$_1$**).

As would be expected from the above-mentioned open- and closed-channel blockade, the pharmacological profile of nAChR inhibition by Ttc followed a non-competitive pattern (**Figure 3B**). Therefore, the extent of I_{ACh} inhibition was independent of agonist concentration (**Figure 3C**), although it was affected by the timing of Ttc application (direct co-application ACh and Ttc *vs.* pre-application of Ttc, followed by its co-application with ACh). Interestingly, when 0.7 μM Ttc was pre-applied alone, the I_{ACh} inhibition elicited either at −60 or +40 mV, showed almost no recovery during the following 32 s pulse of ACh (**Figures 4A$_2$,A$_5$,B$_1$,B$_2$**). We could speculate that Ttc partition in the membrane would account for this slow I_{ACh} recovery. Indeed, protonated Ttc, similar to other molecules with charged ammonium groups, could interact with negatively-charged phosphate groups of membrane phospholipids through long-range coulombic interactions (Pérez-Isidoro et al., 2014). However, membrane adsorption of Ttc at the concentrations used in the present study (below 1 μM) does not seem to sufficiently explain the delayed and long-lasting nAChR blockade found with just pre-application of Ttc. Instead, we think that the sustained nAChR blockade when Ttc was solely pre-applied would be due to Ttc binding outside the channel pore in resting nAChRs (closed-channel blockade), as it was found at both negative and positive potentials (**Figures 4A$_2$,A$_5$**). Accordingly, **Figure 5** shows that Ttc "off" rate kinetics of I_{ACh} (roughly 3 s; **Figure 5C**) is only moderately slower than its corresponding "on" rate (time constant values circa 1.5 s), but much faster than the I_{ACh} recovery observed after Ttc pre-application alone. Furthermore, quaternary ammonium molecules, such as BW284c51 or edrophonium, show similar washout kinetics (in the range of a few seconds) (Olivera-Bravo et al., 2007), even if they are superfused at very different concentrations (0.5 μM and 10 μM for BW284c51 and edrophonium, respectively). Furthermore, Leng et al. (2013) reported the Ttc inhibition of ASIC3 channels by repeating, within the same cell, pH pulses with increasing concentrations of Ttc, up to 30 mM. Despite the high Ttc doses used in that study (over four orders of magnitude above those used in the present study to block nAChRs), no additive effects were apparent when pulses were repeated at 90 s intervals. All of these experimental findings contradict the possibility that the membrane acts as a large reservoir for lipid-partitioned Ttc molecules, which would slowly release Ttc after being washed out from the solution, and thus, sustain nAChR inhibition over time.

When Ttc dose-nAChR inhibition curves were plotted for both I_p and I_{ss} values (**Figure 1C**), they showed that Ttc inhibition was rather similar for both components up to 0.1 μM Ttc. However, at higher concentrations of Ttc, there was increased inhibition at the I_{ss}. This increase in I_{ACh} blockade at its steady state is directly related to the enhancement of I_{ACh} decay, which requires the action of Ttc within the channel pore. Thus, it was not observed when the cell membrane was maintained at positive potentials, which eject the positively charged Ttc from the channel pore (compare recordings of **Figures 4A$_1$,A$_4$**). The acceleration of I_{ACh} decay by Ttc might be mediated by either a slow-pace blockade of nAChRs, enhancement of desensitization, or a combination of both factors. However, we have assembled several experimental findings that support the hypothesis that the main reason is an increase in the rate of nAChR desensitization. First, the same Ttc concentration (0.7 μM) accelerated I_{ACh} decay more sharply when it was co-applied with 100 μM ACh ($\tau_{Ttc} = 0.6$ s) than with 10 μM ACh ($\tau_{Ttc} = 1.0$ s) (**Figure 6**). Second, as already mentioned, Ttc at its IC_{50} blocked nAChRs at both negative and positive potentials, but I_{ACh} decay was only enhanced when the cell was maintained at negative potentials (**Figures 4A$_1$,A$_4$**). Third, the Ttc blocking kinetics was faster than the acceleration of I_{ACh} decay induced by Ttc. Thus, the time course of the voltage-dependent blockade

of nAChR by 0.7 μM Ttc was faster (**Figure 2C**) than the I_{ACh} decay evoked by the same concentration of Ttc, even when co-applied with a high concentration of ACh (100 μM; τ_{Ttc} = 0.6 s, **Figure 6**). Fourth, if Ttc would accelerate I_{ACh} decay because of a slow-pace blockade of nAChRs, it should be detected at all concentrations of Ttc that induce I_{ACh} inhibition. However, 0.1 μM Ttc, which inhibits roughly 25% I_{ACh} (**Figures 1**, **7**), does not modify I_{ACh} decay (**Figure 7**). Fifth, at Ttc concentrations above 0.5 μM, the ratio I_{ss}/I_p vs. its corresponding control value (in the presence of 10 μM ACh alone) is significantly smaller than 1 (**Figure 8B**), indicating an enhancement of nAChR desensitization (Sobolevsky et al., 1999). In contrast, below 0.5 μM Ttc, this quotient is close to 1 (**Figure 8B**). Sixth, Ttc decelerated I_{ACh} deactivation (**Figure 9**). The pronounced deceleration of I_{ACh} deactivation elicited by Ttc, when applied at its IC_{50}, also indicates an enhancement of nAChR desensitization, because of the higher affinity of the desensitized nAChR to the agonist, as previously suggested for $GABA_A$Rs (Jones and Westbrook, 1995). Nevertheless, the solution exchange kinetics of our experimental model limits the temporal resolution to roughly 1.4 s (**Figure 5**). Therefore, to assess the kinetics of the voltage-dependent I_{ACh} blockade, the cell membrane potential was jumped from positive to negative voltages in the presence of Ttc, which facilitated the measurement of this kinetics independently of the solution exchange rate (**Figure 2**). However, as I_{ACh} deactivation kinetics is affected by the solution exchange rate, we referred to the observed values as apparent deactivation time constants, to indicate this limitation.

Altogether, the aforementioned results indicate that Ttc indeed enhances nAChR desensitization. Furthermore, both our functional and virtual docking results support the notion that Ttc accelerates nAChR desensitization by binding to M2 residues located at the interphase between the ECD and TMD (site 2 of **Table 2**), a region that is relevant to the determination of both the open-channel lifetime and rate of desensitization of Cys-loop receptors (Bouzat et al., 2008). Thus, our functional studies indicate that Ttc requires binding within the channel to boost desensitization, as I_{ACh} decay is not affected by Ttc at positive membrane potentials, which eject Ttc from the channel lumen. Consistent with these findings, our docking assays indicated that Ttc binds to residues of the α and γ subunits located at a very shallow depth within the channel pore (**Figures 10Aa_2,B** and **Tables 1**, **2**), both in the open and closed states. Interestingly, one of these residues is αE262, which is located at the extracellular end of the channel pore. This residue is highly conserved among different nAChRs subtypes and has been involved in the desensitization/resensitization of *Torpedo* nAChRs (Forman et al., 2007). Indeed, αE262 mutants have the fast component of nAChR desensitization altered, and photomodification of αE262 with 3-azioctanol stabilizes the desensitized state (Forman et al., 2007). In addition, crystal violet, a nAChR antagonist, reportedly enhances the desensitization of resting receptors, likely by binding to αE262, and stabilizes the desensitized state (Arias et al., 2006). Notably, Ttc inhibits crystal violet binding to resting AChRs (Arias et al., 2006), suggesting that both molecules interact at the same, or nearby sites. However, in our hands, Ttc did not promote changes in desensitization when acting on resting nAChR, as the I_{ACh} decay was not accelerated by the sole pre-application of Ttc, i.e., when Ttc acted on resting receptors only. Moreover, if Ttc had desensitized resting nAChRs, a slow increase of the I_{ACh} would be expected during the subsequent ACh application, because of the slow recovery of nAChR from desensitization; however, no changes in I_{ACh} decay were observed with this protocol (**Figure 4A$_2$**). In contrast, Ttc binding to site 2 enhances nAChR desensitization when the channel is in the open conformation, as evidenced by the accelerated I_{ACh} decay observed when Ttc and ACh were co-applied, either directly, or following a 12 s pre-application of Ttc (**Figures 4A$_1$,A$_3$**). Interestingly, this superficial binding site in the channel pore differs from another, more deeply located within the channel (site 3), to which Ttc binds with higher affinity, thereby eliciting open-channel blockade (steric blockade; **Figure 10**). Nevertheless, our docking assays used the structural models of *Torpedo* nAChR derived from cryo-eletron microscopy as a template, which bears a rather low resolution, particularly in the open-channel model (6.2 Å) (Unwin, 1995). Moreover, these templates contain an error in the TMD alignment that is mainly associated with a shift of one helix turn at the base of the M1-M2 helices. Nevertheless, this TMD region does not appear to be a target of Ttc, neither when the original *Torpedo* templates were used, nor when the homomeric α_7 nAChR refined structure was used (Newcombe et al., 2018). This suggests that the inaccuracies of the original *Torpedo* structural model do not substantially affect the docking results presented. Thus, our virtual docking assays provide a coherent explanation of our experimental observations, in terms of the involvement of different sets of Ttc binding sites that account for its complex modulating actions on nAChRs.

In conclusion, our present results indicate that Ttc, a molecule that is widely used in clinical practice for both topical and spinal administration, should no longer be considered only as a non-competitive blocker of nAChRs that selectively act on the resting (closed) state (Middleton et al., 1999). Here, we provide strong functional evidence indicating that Ttc is a very powerful blocker of muscle-type nAChRs, with an IC_{50} in the submicromolar range, which acts on both the closed and open states of nAChRs. Furthermore, Ttc greatly enhances nAChR desensitization, most likely by binding to the most superficial region of the pore when the channel is in the open conformation. It is worth noting that as around 100 μM Ttc is required to inhibit 80% of voltage-dependent Na^+ channels (Wang et al., 1996), the high potency of Ttc inhibiting muscle-type nAChRs, and perhaps other neuronal subtypes of nAChRs, might explain some of its serious side effects, despite the fact that it is rapidly hydrolyzed by plasma esterases (Moriya, 2005). Nevertheless, Ttc concentrations in plasma of up to 0.7 μM have been reported in humans after its topical application on the skin (2 g, 5% w/w), without any remarkable side effects (Mazumdar et al., 1991). Although roughly all Ttc molecules in physiological solutions are protonated, in contrast to other LAs with amine groups, Ttc binds to different nAChR loci, which accounts for the heterogeneity of its functional effects on nAChRs. These results contribute to a better understanding of the complex modulation

of muscle-type nAChRs by Ttc, and they provide new insights about the key nAChR loci involved in both allosteric and steric modulation.

AUTHOR CONTRIBUTIONS

All authors listed have made a substantial, direct and intellectual contribution to the work, and approved it for publication.

FUNDING

This work was supported by grants BFU2012-31359, SAF2015-66275-C2-1-R, and SAF2017-82977-P (AEI/FEDER, UE) from MINECO and PROMETEO/2014/11 from Generalitat Valenciana (Spain). RC held a predoctoral fellowship from Universidad de Alicante (FPUUA36).

ACKNOWLEDGMENTS

We thank Mr. Simón Moya for expert technical assistance.

SUPPLEMENTARY MATERIAL

The Supplementary Material for this article can be found online at: https://www.frontiersin.org/articles/10.3389/fnmol.2018.00193/full#supplementary-material

REFERENCES

Adams, P. R. (1977). Voltage-jump analysis of procaine action at frog end-plate. *J. Physiol.* 268, 291–318. doi: 10.1113/jphysiol.1977.sp011858

Alberola-Die, A., Fernández-Ballester, G., González-Ros, J. M., Ivorra, I., and Morales, A. (2016a). Muscle-type nicotinic receptor blockade by diethylamine, the hydrophilic moiety of lidocaine. *Front. Mol. Neurosci.* 9:12. doi: 10.3389/fnmol.2016.00012

Alberola-Die, A., Fernández-Ballester, G., González-Ros, J. M., Ivorra, I., and Morales, A. (2016b). Muscle-type nicotinic receptor modulation by 2,6-dimethylaniline, a molecule resembling the hydrophobic moiety of lidocaine. *Front. Mol. Neurosci.* 9:127. doi: 10.3389/fnmol.2016.00127

Alberola-Die, A., Martínez-Pinna, J., González-Ros, J. M., Ivorra, I., and Morales, A. (2011). Multiple inhibitory actions of lidocaine on Torpedo nicotinic acetylcholine receptors transplanted to Xenopus oocytes. *J. Neurochem.* 117, 1009–1019. doi: 10.1111/j.1471-4159.2011.07271.x

Alberola-Die, A., Reboreda, A., Lamas, J. A., and Morales, A. (2013). Lidocaine effects on acetylcholine-elicited currents from mouse superior cervical ganglion neurons. *Neurosci. Res.* 75, 198–203. doi: 10.1016/j.neures.2013.01.005

Albuquerque, E. X., Pereira, E. F. R., Alkondon, M., and Rogers, S. W. (2009). Mammalian acetylcholine receptors: from structure to function. *Physiol. Rev.* 89, 73–120. doi: 10.1152/physrev.00015.2008

Arias, H. R. (1999). Role of local anesthetics on both cholinergic and serotonergic ionotropic receptors. *Neurosci. Biobehav. Rev.* 23, 817–843. doi: 10.1016/S0149-7634(99)00020-2

Arias, H. R., Bhumireddy, P., Spitzmaul, G., Trudell, J. R., and Bouzat, C. (2006). Molecular mechanisms and binding site location for the noncompetitive antagonist crystal violet on nicotinic acetylcholine receptors. *Biochemistry* 45, 2014–2026. doi: 10.1021/bi051752e

Blanchard, S. G., Elliott, J., and Raftery, M. A. (1979). Interaction of local anesthetic with Torpedo californica membrane-bound acetylcholine receptor. *Biochemistry* 18, 5880–5885. doi: 10.1021/bi00593a019

Bouzat, C., Bartos, M., Corradi, J., and Sine, S. M. (2008). The interface between extracellular and transmembrane domains of homomeric Cys-loop receptors governs open-channel lifetime and rate of desensitization. *J. Neurosci.* 28, 7808–7819. doi: 10.1523/JNEUROSCI.0448-08.2008

Changeux, J. P. (2014). Protein dynamics and the allosteric transitions of pentameric receptor channels. *Biophys. Rev.* 6, 311–321. doi: 10.1007/s12551-014-0149-z

Cobo, R., Alberola-Die, A., Mannavola, L., Perez-Rodriguez, R., Soriano, S., Ivorra, I., et al. (2014). Desensitization of muscle-type nicotinic receptors is markedly increased by tetracaine. *Acta Physiol.* 212:26.

Duan, Y., Wu, C., Chowdhury, S., Lee, M. C., Xiong, G., Zhang, W., et al. (2003). A point-charge force field for molecular mechanics simulations of proteins based on condensed-phase quantum mechanical calculations. *J. Comput. Chem.* 24, 1999–2012. doi: 10.1002/jcc.10349

Eterović, V. A., Li, L., Ferchim, P. A., Lee, Y. H., Hann, R. M., Rodriguez, A. D., et al. (1993). The ion channel of muscle and electric organ acetylcholine receptors: differing affinities for noncompetitive inhibitors. *Cell. Mol. Neurobiol.* 13, 111–121. doi: 10.1007/BF00735368

Forman, S. A., Zhou, Q. L., and Stewart, D. S. (2007). Photoactivated 3-azioctanol irreversibly desensitizes muscle nicotinic ACh receptors via interactions at αE262. *Biochemistry* 46, 11911–11918. doi: 10.1021/bi701287a

Gage, P. W., and Wachtel, R. E. (1984). Some effects of procaine at the toad end-plate are not consistent with a simple channel blocking model. *J. Physiol.* 346, 331–339. doi: 10.1113/jphysiol.1984.sp015025

Gallagher, M. J., and Cohen, J. B. (1999). Identification of amino acids of the Torpedo nicotinic acetylcholine receptor contributing to the binding site for the noncompetitive antagonist [3H]tetracaine. *Mol. Pharmacol.* 56, 300–307. doi: 10.1124/mol.56.2.300

Gentry, C. L., and Lukas, R. J. (2001). Local anesthetics noncompetitively inhibit function of four distinct nicotinic acetylcholine receptor subtypes. *J. Pharmacol. Exp. Ther.* 299, 1038–1048.

Gotti, C., and Clementi, F. (2004). Neuronal nicotinic receptors: from structure to pathology. *Prog. Neurobiol.* 74, 363–396. doi: 10.1016/j.pneurobio.2004.09.006

Guex, N., and Peitsch, M. C. (1997). SWISS-MODEL and the Swiss-PdbViewer: an environment for comparative protein modeling. *Electrophoresis* 18, 2714–2723. doi: 10.1002/elps.1150181505

Hurst, R., Rollema, H., and Bertrand, D. (2013). Nicotinic acetylcholine receptors: from basic science to therapeutics. *Pharmacol. Therapeut.* 137, 22–54. doi: 10.1016/j.pharmthera.2012.08.012

Ikeda, S. R., Aronstam, R. S., Daly, J. W., Aracava, Y., and Albuquerque, E. X. (1984). Interactions of bupivacaine with ionic channels of the nicotinic receptor. Electrophysiological and biochemical studies. *Mol. Pharmacol.* 26, 293–303.

Ivorra, I., Fernández, A., Gal, B., Aleu, J., González-Ros, J. M., Ferragut, J. A., et al. (2002). Protein orientation affects the efficiency of functional protein transplantation into the Xenopus oocyte membrane. *J. Membr. Biol.* 185, 117–127. doi: 10.1007/s00232-001-0118-x

Jones, M. V., and Westbrook, G. L. (1995). Desensitized states prolong GABAA channel responses to brief agonist pulses. *Neuron* 15 , 181–191. doi: 10.1016/0896-6273(95)90075-6

Katz, B., and Miledi, R. (1975). The effect of procaine on the action of acetylcholine at the neuromuscular junction. *J. Physiol.* 249, 269–284. doi: 10.1113/jphysiol.1975.sp011015

Koblin, D. D., and Lester, H. A. (1979). Voltage-dependent and voltage-independent blockade of acetylcholine receptors by local anesthetics in Electrophorus electroplaques. *Mol. Pharmacol.* 15, 559–580.

Krieger, E., Darden, T., Nabuurs, S. B., Finkelstein, A., and Vriend, G. (2004). Making optimal use of empirical energy functions: force-field parameterization in crystal space. *Proteins* 57, 678–683. doi: 10.1002/prot.20251

Krieger, E., Koraimann, G., and Vriend, G. (2002). Increasing the precision of comparative models with YASARA NOVA; a self-parameterizing force field. *Proteins* 47, 393–402. doi: 10.1002/prot.10104

Kusano, K., Miledi, R., and Stinnakre, J. (1982). Cholinergic and catecholaminergic receptors in the Xenopus oocyte membrane. *J. Physiol.* 328, 143–170. doi: 10.1113/jphysiol.1982.sp014257

Leng, T., Lin, J., Cottrell, J. E., and Xiong, Z. G. (2013). Subunit and frequency-dependent inhibition of acid sensing ion channels by local anesthetic tetracaine. *Mol. Pain*. 9:27. doi: 10.1186/1744-8069-9-27

Mazumdar, B., Tomlinson, A. A., and Faulder, G. C. (1991). Preliminary study to assay plasma amethocaine concentrations after topical application of a new local anaesthetic cream containing amethocaine. *Br. J. Anest*. 67, 432–436. doi: 10.1093/bja/67.4.432

Middleton, R. E., Strnad, N. P., and Cohen, J. B. (1999). Photoaffinity labeling the Torpedo nicotinic acetylcholine receptor with [3H]tetracaine, a nondesensitizing noncompetitive antagonist. *Mol. Pharmacol.* 56, 290–299. doi: 10.1124/mol.56.2.290

Morales, A., Aleu, J., Ivorra, I., Ferragut, J. A., González-Ros, J. M., and Miledi, R. (1995). Incorporation of reconstituted acetylcholine receptors from Torpedo into the Xenopus oocyte membrane. *Proc. Natl. Acad. Sci. U.S.A.* 92, 8468–8472. doi: 10.1073/pnas.92.18.8468

Morales, A., and Sumikawa, K. (1992). Desensitization of junctional and extrajunctional nicotinic ACh receptors expressed in Xenopus oocytes. *Brain Res. Mol. Brain Res.* 16, 323–329. doi: 10.1016/0169-328X(92)90242-4

Moriya, F. (2005). "Local anesthetics," in *Drugs and Poisons in Humans. A Handbook of Practical Analysis,* eds O. Suzuki and K. Watanabe (Berlin; Heidelberg: Springer-Verlag), 377–389. doi: 10.1007/3-540-27579-7_41

Morris, G. M., Huey, R., and Olson, A. J. (2008). Using AutoDock for ligand receptor docking. *Curr. Protoc. Bioinformatics* Chapter 8:Unit 8.14. doi: 10.1002/0471250953.bi0814s24

Nayak, T. K., Purohit, P. G., and Auerbach, A. (2012). The intrinsic energy of the gating isomerization of a neuromuscular acetylcholine receptor channel. *J. Gen. Physiol.* 139, 349–358. doi: 10.1085/jgp.201110752

Neher, E., and Steinbach, J. H. (1978). Local anaesthetics transiently block currents through single acetylcholine-receptor channels. *J. Physiol.* 277, 153–176. doi: 10.1113/jphysiol.1978.sp012267

Newcombe, J., Chatzidaki, A., Sheppard, T. D., Topf, M., and Millar, N. S. (2018). Diversity of nicotinic acetylcholine receptor positive allosteric modulators revealed by mutagenesis and a revised structural model. *Mol. Pharmacol.* 93, 128–140. doi: 10.1124/mol.117.110551

Ogden, D. C., Siegelbaum, S. A., and Colquhoun, D. (1981). Block of acetylcholine-activated ion channels by an uncharged local anaestethic. *Nature* 289, 596–598. doi: 10.1038/289596a0

Olivera-Bravo, S., Ivorra, I., and Morales, A. (2005). The acetylcholinesterase inhibitor BW284c51 is a potent blocker of Torpedo nicotinic AchRs incorporated into the Xenopus oocyte membrane. *Br. J. Pharmacol.* 144, 88–97. doi: 10.1038/sj.bjp.0705965

Olivera-Bravo, S., Ivorra, I., and Morales, A. (2007). Diverse inhibitory actions of quaternary ammonium cholinesterase inhibitors on Torpedo nicotinic ACh receptors transplanted to Xenopus oocytes. *Br. J. Pharmacol.* 151, 1280–1292. doi: 10.1038/sj.bjp.0707329

Parikh, V., Kutlu, M. G., and Gould, T. J. (2016). nAChR dysfunction as a common substrate for schizophrenia and comorbid nicotine addiction: current trends and perspectives. *Schizophr. Res.*. 171, 1–15. doi: 10.1016/j.schres.2016.01.020

Pérez-Isidoro, R., Sierra-Valdez, F. J., and and. Ruiz-Suárez, J. C. (2014). Anesthetic diffusion through lipid membranes depends on the protonation. *Sci. Rep.* 4:7534. doi: 10.1038/srep07534

Schulte, M. K., Khatri, S., Huang, Y., DeCristofano, L., and LeBlanc, G. G. (2016). Allosteric modulation and potential therapeutic applications of heteromeric nicotinic acetylcholine receptors. *Neurotransmitter* 3:e1275. doi: 10.14800/nt.1275

Sobolevsky, A. I., Koshelev, S. G., and Khodorov, B. I. (1999). Probing of NMDA channels with fast blockers. *J. Neurosci.* 19, 10611–10626. doi: 10.1523/JNEUROSCI.19-24-10611.1999

Spitzmaul, G., Gumilar, F., Dilger, J. P., and Bouzat, C. (2009). The local anaesthetics proadifen andadiphenine inhibit nicotinic receptors by different molecular mechanisms. *Br. J. Pharmacol.* 157, 804–817. doi: 10.1111/j.1476-5381.2009.00214.x

Steinbach, A. B. (1968). Alteration by Xilocaine (lidocaine) and its derivatives of the time course of the end plate potential. *J. Gen. Physiol.* 52, 144–161. doi: 10.1085/jgp.52.1.144

Sugiyama, K., and Muteki, T. (1994). Local anesthetics depress the calcium current of rat sensory neurons in culture. *Anesthesiology* 80, 1369–1378. doi: 10.1097/00000542-199406000-00025

Taly, A., Corringer, P. J., Guedin, D., Lestage, P., and Changeux, J. P. (2009). Nicotinic receptors: allosteric transitions and therapeutic targets in the nervous system. *Nat. Rev. Drug Discov.* 8, 733–750. doi: 10.1038/nrd2927

Unwin, N. (1995). Acetylcholine receptor channel imaged in the open sate. *Nature* 373, 37–43. doi: 10.1038/373037a0

Unwin, N. (2005). Refined structure of the nicotinic acetylcholine receptor at 4 Å resolution. *J. Mol. Biol.* 346, 967–989. doi: 10.1016/j.jmb.2004.12.031

Unwin, N., and Fujiyoshi, Y. (2012). Gating movement of Acetylcholine receptor caught by plunge-freezing. *J. Mol. Biol.* 422, 617–634. doi: 10.1016/j.jmb.2012.07.010

Wang, G. K., Vladimirov, M., Quan, C., Mok, W. M., Thalhammer, J. G., and Anthony, D. C. (1996). N-butyl tetracaine as a neurolytic agent for ultralong sciatic nerve block. *Anesthesiology* 85, 1386–1394. doi: 10.1097/00000542-199612000-00020

Wang, H., Zhang, Y., and Li, S. (2010). The effect of local anesthetics on the inhibition of adult muscle-type nicotinic acetylcholine receptors by nondepolarizing muscle relaxants. *Eur. J. Pharmacol.* 630, 29–33. doi: 10.1016/j.ejphar.2009.12.028

Woodhull, A. M. (1973). Ionic blockage of sodium channels in nerve. *J. Gen. Physiol.* 61, 687–708. doi: 10.1085/jgp.61.6.687

Wu, Z. S., Cheng, H., Jiang, Y., Melcher, K., and Xu, H. E. (2015). Ion channels gated by acetylcholine and serotonin: structures, biology, and drug discovery. *Acta Pharmacol. Sin.* 36, 895–907. doi: 10.1038/aps.2015.66

Zucchi, R., and Ronca-Testoni, S. (1997). The sarcoplasmic reticulum Ca^{2+} channel/ryanodine receptor: modulation by endogenous effectors, drugs and disease states. *Pharmacol. Rev.* 49, 1–51.

Conflict of Interest Statement: The authors declare that the research was conducted in the absence of any commercial or financial relationships that could be construed as a potential conflict of interest.